

DUST IN THE PHOTOSPHERIC ENVIRONMENT: UNIFIED CLOUDY MODELS OF M, L, AND T DWARFS

TAKASHI TSUJI

*Institute of Astronomy, The University of Tokyo,
Mitaka, Tokyo, 181-0015, Japan*

ttsuji@ioa.s.u-tokyo.ac.jp

ABSTRACT

We report an attempt of constructing unified cloudy models for M, L, and T dwarfs. For this purpose, we first discuss opacities as well as thermochemical properties of the cool and dense matter. Below about 2000 K, refractory material condenses and dust will play a major role as a source of opacity. Then a major problem in modeling the photospheres of very cool dwarfs is how to treat dust, and especially how dust could be sustained in the static photosphere for a long time. Under the high density of the photospheres of cool dwarfs, dust forms easily at the condensation temperature, T_{cond} , but the dust will soon grow larger than its critical radius r_{cr} (at which the Gibbs free-energy of condensation attains the maximum) at the critical temperature T_{cr} . Such large dust grains with $r_{\text{gr}} \gtrsim r_{\text{cr}}$ will soon segregate from the gas and precipitate below the photosphere. For this reason, dust exists effectively only in the limited region of $T_{\text{cr}} \lesssim T \lesssim T_{\text{cond}}$ in the photosphere, and this means that a dust cloud is formed deep in the photosphere rather than in the cooler surface region. With this simple model of dust cloud, we show that the non-grey model photosphere in radiative-convective equilibrium can be extended to T_{eff} as low as 800 K. Since $T_{\text{cond}} \approx 2000$ K for the first condensates such as corundum and iron, the dust cloud is rather warm and necessarily located deeper in the photosphere ($\tau > 1$) for the cooler objects (note that $T \approx T_{\text{eff}}$ at $\tau \approx 1$). This explains why dust apparently shows little observable effect in T dwarfs. For warmer objects, the dust cloud which is always formed at the same temperature range of $T_{\text{cr}} \lesssim T \lesssim T_{\text{cond}}$ can be located nearer the surface ($\tau < 1$) and, for this reason, L dwarfs appear to be dusty. We show that the recently proposed spectral classification of L and T dwarfs can consistently be interpreted by a single grid of our unified cloudy models with the thin dust cloud deep in the photosphere.

Subject headings: molecular processes — stars: atmospheres — stars: late-type — stars: low-mass, brown dwarfs — stars: spectral classification —

1. INTRODUCTION

The present stellar spectral classification in terms of O, B, A, F, G, K, and M (with branching into R-N and S) has been used since the beginning of the 20th century. For most of these spectral types, the modeling of stellar photospheres has now matured enough within the framework of the so-called classical theory of stellar photospheres in general (e.g. Kurucz 1994). In the case of the latest M, S, and C types, however, the progress in modeling photospheres was rather slow largely because of the extreme

complexity of opacities dominated by molecules (e.g. Gustafsson & Jørgensen 1994). As for cool dwarfs, some initial attempts to include molecular line opacities such as of H₂O were done a long time ago (e.g. Auman 1969; Tsuji 1969), and a systematic study of M dwarf model photospheres including several molecular opacity sources has been done by Mould (1976) who provided a large grid for M (sub) dwarfs for the first time.

More recent interest in cool dwarfs was motivated by the progress of observations on faint cool dwarfs on one hand and by the increased interest on the so-called brown dwarfs on the other. The possible presence of such substellar objects was conceived a long time ago and their basic properties were predicted already in the 1960's (e.g. Hayashi & Nakano 1963; Kumar 1963). Serious searches for brown dwarfs required accurate predictions of observable properties and hence of the atmospheric structures of brown dwarfs (e.g. Burrows & Liebert 1993). Some attempts to extend the model photospheres to the substellar regime with T_{eff} as low as 1000 K have been done by Saumon et al. (1994) for the case of zero metallicity and by Tsuji & Ohnaka (1995a) for the solar as well as some sub-solar metallicities in the same low temperature regime. These works revealed the importance of some new opacity sources such as H₂ collision-induced absorption (CIA) and methane (CH₄) under the extreme condition of the cool and dense photospheres. Also, many model photospheres for a large parameter space were extended to T_{eff} as low as 1500 K by Allard & Hauschildt (1995) and to the M dwarf regime by Brett (1995).

While gas phase chemistry has been sufficient in interpreting the classical spectral types from O to M, dust should be the major ingredient in the very cool dwarfs. This possibility was first noted on the late M dwarfs (Tsuji, Ohnaka, & Aoki 1996a) and confirmed on a larger sample of M dwarfs (Jones & Tsuji 1997). However, the cool genuine brown dwarf Gl 229B finally discovered by Nakajima et al. (1995) revealed no evidence for dust but showed strong bands of volatile molecules such as methane and water (Oppenheimer et al. 1995). Such a result was quite consistent with the detailed thermochemical equilibrium calculations by Fegley & Lodders (1996) who first showed that refractory elements including Ca, Al, Ti, V, Mg, Si, Fe are removed by condensate cloud formation from the observable photosphere and hence should not be observed. In fact, the spectra of Gl 229B could rather be well interpreted by the dust-free model developed before the discovery of Gl 229B (Tsuji & Ohnaka 1995a), while brown dwarf candidate GD 165B discovered by Becklin & Zuckerman (1988) could first be explained by the dusty models (Tsuji et al. 1996b). Models of Gl 229B by other authors (e.g. Allard et al. 1996; Marley et al. 1996) also showed little effect of dust, and further extended to the regime of giant planets (Burrows et al. 1997).

Meanwhile progress in observations of ultracool dwarfs was marvelous: Many new objects cooler than M dwarfs were discovered with the DEep Near-Infrared Sky survey (DENIS; Delfosse et al. 1997) as well as with the Two Micron All Sky Survey (2MASS; Kirkpatrick et al. 1997) and the newly detected cool dwarfs were named as L dwarfs. Cooler brown dwarf similar to Gl 229B, named as T dwarf, was more difficult to find but several T dwarfs were finally discovered with the 2MASS (Burgasser et al. 1999, 2000a,b) and with the Sloan Digital Sky Survey (SDSS; Strauss et al. 1999; Tsvetanov et al. 2000). As is usually the case in the new field opened with the discovery of new objects, a great deal of effort has been done on how to classify the newly defined L and T dwarfs. Initial attempts include detailed classifications of L dwarfs by Kirkpatrick et al. (1999, 2000) and by Martín et al. (1999) based on the optical spectra. More recently, classification of L dwarfs was extended with the use of the near infrared spectra (e.g. Reid et al. 2001; Testi et al. 2001). The first attempt on the detailed classification of T dwarfs was done by Burgasser et al. (2002), and a unified classification scheme for L and T dwarfs was proposed by Geballe et al. (2002). Now, a major question is what is the exact meaning of the new spectral classification in terms of L and T types.

Dust should certainly play a crucial role in interpreting the spectra of ultracool dwarfs, but a major problem is how dust could be sustained in the photosphere for a long time. In fact, dust may easily segregate from the gas and precipitate below the observable photosphere if dust grains grow larger, and Gl 229B may represent such a case. On the other hand, late M dwarfs and GD 165B may represent a case that dust grains can be sustained in the photosphere. Thus, we have considered two extreme cases to explain different types of ultracool dwarfs as reviewed elsewhere (Tsuji 2000); dusty model in which dust grains are sustained throughout the photosphere (case B) and dust-segregated model in which all the dust grains have precipitated below the observable photosphere (case C). Recently, more or less similar cases showing the limiting effect of dust were discussed by Allard et al. (2001). However, new observations on a larger sample of L and T dwarfs revealed difficulty of the simple dusty and dust segregated models, and suggested a more realistic model somewhere in between these two extreme cases (e.g. Tinney 1999).

It took sometime before we noticed that the extreme models, in which the photosphere is filled with dust (case B) or fully depleted of dust (case C), are physically unrealistic. We then considered dust formation and segregation in a single model, the necessarily consequence of which was the presence of a warm dust cloud deep in the photosphere. This model was first applied to a limited purpose of explaining the large optical flux depression observed in the apparently dust-free T dwarf Gl 229B (Tsuji, Ohnaka, & Aoki 1999). Although the optical flux depression itself may be explained by the strong alkali metal lines, as also noted by Burrows, Marley, & Sharp (2000), the basic idea of the warm dust cloud deep in the photosphere includes an important implication to be developed to a unified model photosphere of ultracool dwarfs (Tsuji 2001). We now examine such a possibility in detail in this paper.

Recently, the dust cloud model discussed in connection with the planetary atmospheres has been extended to brown dwarfs (e.g. Lunine et al. 1989; Ackerman & Marley 2001; Marley et al. 2002). Since brown dwarfs are just in between stars and planets, approaches from both the stellar and planetary sides should be useful and even complementary to each other. In the present paper, however, we purposely restricted ourselves to the stellar approach and we hope to show how the methodology of non-grey radiative-convective model stellar photosphere could be extended to the photosphere of substellar objects.

2. THERMOCHEMISTRY

The most important basic input data, the composition of the chemical elements, is by no means well established yet even for the Sun to which we referred (Sect. 2.1). For model photospheres of ultracool dwarfs including brown dwarfs, the equation of state (EOS) should be solved down to $T \approx 500$ K, and we assume that the ideal gas law can be applied up to the density regime of Kbar (1 Kbar = 10^9 dyn cm $^{-2}$ $\approx 10^3$ atms) (Sect. 2.2). Under the high density of the photospheres of cool dwarfs, the thermodynamical equilibrium can be well realized, and not only molecules but also dust grains are treated under the assumption of the local thermodynamical equilibrium (LTE) (Sect. 2.3).

2.1. Chemical Composition

For ultracool dwarfs of the disk population, we may assume the chemical composition of the solar system, for which the result by Anders & Grevesse (1989) is widely used. However, the solar system

abundance is by no means well established yet and several revisions are needed (e.g. Lodders & Fegley 1998). For example, the iron abundance should be represented by the meteoritic abundance, which was confirmed to be the same with the solar photospheric abundance at last (Biémont et al. 1991; Holweger et al. 1991). Recently, a more drastic revision is proposed for the solar oxygen abundance: $\log A_O = 8.69 \pm 0.05$ (Allende Prieto, Lambert, & Asplund 2001) on the scale of $\log A_H = 12.0$ against the higher value of $\log A_O = 8.92$ (Anders & Grevesse 1989). The revised oxygen abundance is more consistent with the other disk population objects, but this problem should deserve further detailed analyses. Especially, the revised oxygen abundance and a slightly updated carbon abundance of $\log A_C = 8.60$ (Grevesse et al. 1991) are rather close and a difficult problem appears as will be discussed in Sect.7.3. In the present work, we consider 34 elements of the solar system mixture summarized in Table 1, which is still based on Anders & Grevesse (1989) except for minor changes footnoted in the Table, but we must remember that the solar abundances are by no means well established yet. We also computed some models with the new (low) oxygen abundance, and the results will be used to see the effect of oxygen abundance in Sect.7.3.

At the low temperatures and high densities realized in the photospheres of ultracool dwarfs, most compounds formed from H, C, N, O, and S are volatile and the gas phase chemical equilibrium plays a dominant role. On the other hand, other abundant elements such as Mg, Fe, Si, and Al condense in refractory compounds and phase transitions from gas to solid play a major role. These 9 elements, together with the inert He, Ne, and Ar, constitute the most abundant elements in the solar system mixture and play a major role in determining the physical and chemical properties of the gaseous mixtures of the similar compositions.

2.2. Gas Phase Chemical Equilibrium

After a survey of about 600 species in the chemical equilibria of 34 elements (Tsuji 1973), we selected about 100 species in solving the chemical equilibrium during the iterations of modeling the photospheres. The thermochemical data used are mostly unchanged except for controversial cases such as FeH (see Appendix), but some thermodynamical data should certainly be updated as pointed out by Lodders & Fegley (2002). For the purpose of the present work, however, we hope that the thermodynamical data of abundant molecules which are important as sources of opacity are relatively well established.

One important change from the chemical equilibrium familiar in stellar photospheres is that CO is no longer the major species of carbon and that this role is taken over by CH₄ at temperatures below about 1000 K in dense photospheres even for the case of $A_O > A_C$. A belief that all the carbon atoms are used in forming carbon monoxide (CO) in oxygen-rich photospheres is no longer true in the photospheres of substellar objects, and this is simply because CH₄ is thermodynamically more stable than CO at the very low temperature and high density. This fact also implies that oxygen locked in CO is released and available to form additional H₂O. For the same reason, almost entire oxygen is used to form H₂O rather than CO even in the carbon-rich gaseous mixture ($A_O < A_C$) at the high density below about 1000 K. This means that CH₄ and H₂O are the most abundant molecules independently of the oxygen to carbon ratio, and there will be no spectral branching into M, S, and C types in the brown dwarf regime even if some brown dwarfs happen to have chemical peculiarity such as $A_O < A_C$.

Other polyatomics such as NH₃, PH₃, H₂S are also abundant and will play some role as opacity sources. Although the gas phase chemical equilibrium in oxygen-rich photospheres is relatively simple

even at very low temperature and high pressure, some interesting features are to be noted. For example, a stable negative molecular ion such as SH^- appears as a sink of free electrons. It is to be noted, however, that the abundances of most volatile molecules remain unchanged by the formation of refractory condensates.

2.3. Condensation

The phase transition from gas to solid in chemical equilibrium has been discussed in the 1960's (e.g. Lord 1965; Larimer 1967) for the first time. Since then, detailed studies of condensation have been developed in connection with the primitive solar nebula (e.g. Grossman 1972) as well as with the giant planet atmospheres (e.g. Fegley & Lodders 1994). Also, the effect of condensation in molecular equilibrium was extended to the low pressure environments such as stellar envelopes (e.g. Sharp & Huebner 1990). More recently, detailed analyses of the atmospheric chemistry including condensation have been done with direct applications to the brown dwarf atmospheres in mind (Burrows & Sharp 1999; Lodders 1999; Lodders & Fegley 2002).

Although several dozens of condensed species have been treated in the chemical equilibrium by the works just referred to above, we found it not practical to include so many species in our modeling, which requires many iterative processes by itself. Also, it is difficult to specify dust opacity for each individual species accurately at present. For these reasons, we decided to represent the effect of dust formation by the three species, namely corundum (Al_2O_3), iron (Fe), and enstatite (MgSiO_3). In modeling photospheres, the first condensate should be most important since it determines the basic structure of the photosphere with dust and gives a large effect on the next condensates. It is known that the first condensate in the solar composition mixture is ZrO_2 (Fegley & Kornacki 1986; Sharp & Huebner 1990), which, however, is of low concentration because of the low abundance of Zr. The next condensates are Al_2O_3 (at relatively low pressure) or iron (at relatively high pressure) as can be confirmed in Fig.2 of Lodders (1999). These condensates are quite abundant, and we regard corundum and iron as if they are the first condensates in our computation. Also, we represent silicate minerals by MgSiO_3 which condenses at rather low temperatures. Although forsterite (Mg_2SiO_4) condenses at the higher temperature, we regard MgSiO_3 as the representative of the low temperature condensates. Since Fe, Mg, Si, and Al are the most abundant elements that produce refractory condensates, the total amount of condensed species can be approximated by these three species. The resulting condensation lines of corundum, iron, and enstatite are graphically shown in Figs.2-4. These results agree well with those by a more detailed computation by Lodders (1999) (see her Fig.2) for a wide range of the total pressure.

In our simplified treatment, we first solved the gaseous equilibrium and then the chemical equilibrium including condensation was solved for Fe, Mg, Si, and Al. However, the condensation of silicates removes about 15% of oxygen and will change the gaseous equilibrium as noted by Lodders & Fegley (2002). We have confirmed that this effect is very important especially for the case of the low oxygen abundance ($\log A_{\text{O}} = 8.69$), since the oxygen left in the gaseous phase is effectively $\log A_{\text{O}} \approx 8.69 - 0.07 \approx 8.62$ after 15% oxygen is locked in silicate and this is very close to the carbon abundance of $\log A_{\text{C}} = 8.60$. In this case, the gaseous mixture is effectively close to the case of $A_{\text{O}}/A_{\text{C}} \approx 1$, and H_2O abundance shows a drastic decrease while CH_4 abundance show an enhancement. Some details of this effect will be discussed in Sect.7.3. On the other hand, this effect in the case of the high oxygen abundance is just to reduce the oxygen-containing molecules by 0.07 dex at the largest and this effect

will not be so serious for our present modeling as will be shown in Sect.7.3.

As already noted by Fegley & Lodders (1996), refractory elements are removed from the gas phase mixture by the condensation. Such a change in molecular abundances produces drastic effect on opacity if the non-volatile molecules are important sources of opacity. This is actually the case of TiO, VO, FeH, and CaH, for which we have included CaTiO_3 (perovskite), VO, Fe, and $\text{Ca}_2\text{MgSi}_2\text{O}_7$ (akermanite), respectively. This is just to see the approximate effect of condensation on the molecular abundances, and these condensates (except for Fe) are not considered as sources of dust opacities for the reason outlined above. It is to be noted, however, that Ca is the next abundant refractory elements after Al, and we are underestimating the effect of dust opacities.

Chemistry of a less abundant element is generally more complicated because all the compounds composed of elements more abundant than the element must be considered. This is the case of alkali metals such as Na and K which suffer drastic depletions by $\text{NaAlSi}_3\text{O}_8$ and KAlSi_3O_8 , respectively, at true thermal equilibrium, but may remain in atomic forms if highly refractive condensates including Si and Al are removed from the photosphere, as noted by Lodders (1999) and by Burrows (2001). Also, detailed analysis of the alkali metal chemistry by Lodders (1999) showed that sulfides and chlorides should condense below about 1000 K and we considered the condensation of KCl and K_2S . We have used the thermochemical data for KCl and K_2S from the JANAF table (Chase et al. 1985) and we applied the Gibbs free energy of formation by Sharp & Huebner (1990) for other dust species discussed above. The thermodynamical data are still being up-dated and the recent revisions are reviewed by Lodders & Fegley (2002).

3. OPACITIES

At the very low temperature and high density environment to be expected in the photospheres of very low mass objects, new opacity problems appear: First, some polyatomics such as CH_4 and NH_3 must be added to the already known molecular line opacities (e.g. CO, H_2O , TiO, VO etc.) (Sect.3.1). Second, collision-induced absorption (CIA) due to H_2-H_2 and H_2-He pairs plays an increasingly important role at higher densities (Sect.3.2). Third, as soon as various refractory condensates are formed as expected by the thermochemical law, they act as efficient opacity sources over the entire spectral region because of their large extinction cross-sections (Sect.3.3). Fourth, atomic lines should not be neglected, since pressure broadened wings of strong alkali metal lines play a significant role as a source of opacities in cool and dense photospheres (Sect.3.4).

3.1. Molecular Line Opacities

We considered the effect of molecular line absorption by the band model method during the construction of model photospheres, and used detailed linelist to evaluate the final emergent spectra after the model has converged. In the band model method, molecular line opacity is characterized by two parameters, the straight mean absorption cross-section and the mean line separation. Then, we apply the Voigt-Analogue Elsasser Band Model (VAEBM), which consists of an array of Voigt profiles of equal intensity, spaced at equal intervals (Golden 1969). For some cases (e.g. CH_4), however, we applied this method by its simplest form assuming that the line structure is completely smeared out (also known as the Just Overlapping Line Approximation - JOLA) because of the lack of the necessary molecular

data. More details on the formulation of the band model method, together with its applicability and limitation, have been discussed elsewhere (Tsuji 1984, 1994).

We have considered ro-vibration bands of diatomic (CO, OH, SiO) as well as polyatomic (H₂O, H₂S, NH₃, PH₃, CH₄) molecules, together with the pure rotation transitions so far as they are allowed. We have also considered electronic transitions of the refractory molecules including TiO, VO, FeH, CaH, and MgH. The opacity data used are summarized in the Appendix.

3.2. Collision-Induced Absorption (CIA) of H₂

At the very high densities to be expected in the photospheres of ultracool dwarfs, absorption due to the dipole moment induced by collisions should be important for such abundant homo-nuclear molecules as H₂. In this case, individual lines are highly broadened because of the short time of the intermolecular interaction inducing the dipole moment and hence completely smeared out. As a result, the collision-induced absorption (CIA) of H₂ dominates the whole infrared region by quasi-continuous absorption. The importance of H₂ CIA in the photospheres of cool dwarf stars has been recognized at an early time (Linsky 1969; Tsuji 1969), but accurate cross-sections based on the detailed quantum mechanical analysis have been made available only recently by Borysow and her collaborators. The details are discussed for the case of H₂ - He pairs (Borysow & Frommhold 1989; Borysow, Frommhold, & Moraldiet 1989) as well as H₂ - H₂ pair (Borysow & Frommhold 1990; Zheng & Borysow 1995), and more recently by Borysow, Jørgensen, & Zheng (1997). We have reproduced the absorption coefficients with the use of the computer codes kindly made available by Dr. Borysow.

3.3. Dust Opacities

For our present purpose, dust opacities are represented by the three species discussed in Sect.2.3, namely corundum (Al₂O₃), iron (Fe), and enstatite (MgSiO₃). Further, we will show that only small dust grains can be sustained in the photosphere and hence will be important as sources of opacity (Sect.4.1). The mass absorption coefficient of dust grains of radius r_{gr} is

$$\kappa(\text{cm}^2/\text{gram}) = \pi r_{\text{gr}}^2 Q_{\text{abs}} / (4\pi r_{\text{gr}}^3 \rho / 3), \quad (1)$$

where Q_{abs} is the absorption efficiency factor and ρ is the density of the grain. Then, κ depends little on the grain size so far as $r_{\text{gr}} < 0.01\mu\text{m}$, since

$$Q_{\text{abs}} \propto r_{\text{gr}} \quad (2)$$

at $x = 2\pi r_{\text{gr}}/\lambda \ll 1$ (van de Hulst 1957). For this reason, the resulting mass absorption coefficient remains unchanged for any size distribution so long as the grains are small enough, and dust opacities are evaluated for $r_{\text{gr}} \approx 0.01\mu\text{m}$ throughout.

For the grains of sub-micron size, dust opacities can be evaluated by a series expansion of the Mie formula (van de Hulst 1957). We used the optical constants for corundum by Eriksson et al. (1981), who presented the refractive index in the 0.4-2.0 μm wavelength range and the dielectric function in the 5-50 μm range. We have made interpolation or extrapolation for the range where data are missing. For iron, we used the experimental data by Lenham & Treherne (1966) and by Ordal et al. (1988). For

enstatite, we applied the empirical opacity for warm oxygen-deficient circumstellar silicate by Ossenkopf, Hennings, & Mathis (1992). Although silicate abundance is represented by that of enstatite, it actually represents all the silicates as noted in Sect.2.3 and the opacity used also includes many silicates other than enstatite.

It is to be kept in mind that the actual dust opacity may be more complicated. For example, dust opacities under astronomical environment cannot be determined uniquely with the laboratory data, since dust grains in astronomical environment may never consist of pure substance but may be composed of different species. This fact may make the astronomical grains to be rather dirty than clean or to be heterogeneous (e.g. core-mantle structure) rather than homogeneous. Also, dust opacity depends on additional parameters such as shape of the grains (e.g. Alexander & Ferguson 1994). It is not possible, however, to consider all these complexities at present and our dust opacities are very preliminary ones.

3.4. Alkali Metals

Non-refractory elements such as alkali metals remain in mono-atomic gas at low temperatures near 1000 K and their strong resonance lines contribute significantly to suppress the optical radiation observed in cool brown dwarfs such as Gl 229B (Tsuij et al. 1999). The exact evaluation of this rather simple opacity source, however, appear to be difficult because of the uncertainty in the line broadening theory of such strong lines (Burrows et al. 2000). In the present study, we assumed the classical Lorentz line shape, but this should be replaced by a more appropriate formula when it is available in the future.

3.5. Opacities per Gram of Stellar Material

With the absorption cross-section for each species, we evaluate the absorption coefficient per gram of stellar material by solving chemical equilibrium for given temperature and gas pressure. Now, for each spectral mesh, we have the two parameters - the straight mean absorption coefficient κ_i and the mean line separation d_i for i -th species that is important as a line opacity source. Then, the total absorption coefficient for molecular line opacity is simply the sum of κ_i . The average line separation d for the spectral mesh for all the contributing molecules (N species) can be estimated by

$$\frac{1}{d} = \left\{ \sum_{i=1}^N \left(\frac{\kappa_i}{d_i} \right)^{1/2} \right\}^2 / \sum_{i=1}^N \kappa_i. \quad (3)$$

The results are the integrated mass absorption coefficient κ and the average mean line separation d for the given spectral mesh, chemical composition, temperature, and gas pressure. Then, the opacity distribution function (ODF) can be estimated within the framework of the VAEBM, by which line broadenings due to turbulence and collision are considered at each step of integration of the model photosphere. In this way, once the two parameters - κ_i and d_i - for each molecule are prepared, an approximate ODF can easily be estimated for any chemical composition, temperature, gas pressure, and micro-turbulent velocity, during the iterative procedures in construction of model photosphere. An example of the extinction coefficients per gram of stellar material for the chemical composition of Table 1, $T = 1008$ K, and $\log P_g = 6.0$ is shown in Fig. 1. The Rosseland and Planck mean opacities are also evaluated based on these absorption coefficients (e.g. Tsuij & Ohnaka 1995b).

4. MODEL PHOTOSPHERES WITH DUST

Unlike the case of cool giant stars where dust forms in the outflow, dust in cool dwarfs forms in the static photosphere and one problem is how dust could be sustained in the photosphere for a long time. Thus, there should be some fundamental differences in the dust formation mechanisms in low and high luminosity stars. Nevertheless, the basic processes of dust formation should be understood by the same physical principle and we follow a semi-empirical approach based on the homogeneous nucleation theory (Sect.4.1). Then, it can be shown that a dust layer (or may be referred to as a dust cloud) should be formed rather deep in the photosphere as a natural consequence of dust formation and segregation (Sect.4.2). We incorporate the dust cloud in the construction of model photosphere by the application of the classical non-grey theory (Sect.4.3).

4.1. Dust Formation and Segregation in the Photospheric Environment

The thermodynamical condition of condensation is well fulfilled in the photospheres of cool dwarfs (Sect.2.3). This is a necessary condition but not the sufficient condition for condensation, since dust formed in the stellar photosphere is usually in a form of droplet which is subject to decay by the surface tension force. For this reason, dust may form when the super-saturation ratio $S = p/p_{\text{sat}}$ (p_{sat} is the saturation vapor pressure) exceeds unity, but will dissolve as soon as it is formed. The net effect is that effective nucleation does not start even if $S > 1$ and this phenomenon is generally referred to as super-saturation.

In the dense photosphere of cool dwarfs, however, we assume that the nucleation will eventually start sometime after the thermodynamical condition of condensation is fulfilled. According to the classical theory of homogeneous nucleation (e.g. Hasegawa & Kozasa 1988), the equilibrium concentrations of n -mer cluster $C_e(n)$ and monomer $C_e(1)$ are related by

$$C_e(n) = C_1(1) \exp[-\Delta G(n)/kT], \quad (4)$$

where $\Delta G(n)$ is the Gibbs free energy of formation of n -mer given by

$$\Delta G(n) = -nkT \ln S + 4\pi a_0^2 n^{2/3} \sigma, \quad (5)$$

where S is the super-saturation ratio, a_0 is a radius of monomer, and σ is the surface tension of the condensate. The Gibbs free energy of formation $\Delta G(n)$ shows a maximum at $n = n^*$ given by

$$n^* = \frac{8\pi a_0^2 \sigma^3}{3kT \ln S}. \quad (6)$$

Since the Gibbs free energy cannot increase in any chemical process, clusters with $n < n^*$ cannot grow while those with $n > n^*$ can.

This result implies that the cluster can grow stably only if it exceeds the critical radius r_{cr} which corresponds to n^* given by eqn.(6). In other words, stable dust grain can be formed only if the binding force which is proportional to the total number of monomers ($\propto r_{\text{gr}}^3$) exceeds the destructive force due to surface tension which is proportional to the surface area ($\propto r_{\text{gr}}^2$) at $r_{\text{gr}} = r_{\text{cr}}$. For this reason, dust has been regarded as formed when its size exceeds the critical radius in general. For example, in the case of dust formation in the mass-loss outflow from evolved stars, it is indispensable that the dust grows to be

larger than the critical size in the dust forming region before it is ejected to rarefied circumstellar space, since otherwise dust will resolve soon during the outflow and there is no chance for it to be formed again.

In the case of stationary photosphere, however, clusters will grow irreversibly to the larger grains after the cluster size exceeds the critical size. If dust grains are formed in the traditional sense, they will grow further to the more stable larger grains. But such larger grains may be difficult to be sustained in the static photosphere and will finally segregate from the gaseous mixture. Such large grains may no longer be important as sources of opacity, since they will fall below the visible photosphere or may be floating as impurities of a small filling factor in the photosphere. The very fact that cool brown dwarfs such as Gl 229B show little evidence for dust could be explained this way and this fact can be regarded as evidence that dust grains have actually segregated from the ambient gaseous mixture in the photosphere of cool dwarfs (Tsuji et al. 1996b).

On the other hand, if dust grains remain to be smaller than the critical size, they cannot grow to the stable solid particles. This case that dust grains are unstable, however, is very interesting since small dust grains may be destroyed easily but will soon be formed again and *vice versa*, so long as the thermodynamical condition of condensation is fulfilled (i.e. $S > 1$). Thus, small dust grains whose abundance is determined by the chemical equilibrium always present in the static photosphere and dust can be regarded as formed even if its size is below the critical size. The reason why cluster sizes remain within the critical size cannot be known exactly, but the clusters may anyhow be small enough just when they are formed and also they may be destroyed by collisions to each other at the high density of photospheres of cool dwarfs.

In the unstable regime of dust formation where thermal equilibrium is realized, small dust grains are in detailed balance between formation and destruction, and this gives a natural answer why dust grains can be sustained in the static photosphere. In fact, this will explain why some cool dwarfs including late M dwarfs appear to be dusty (e.g. Jones & Tsuji 1997), and further why dust could survive as long as the lifetime of such long-lived stars as M dwarfs. Thus, somewhat paradoxically, a sufficient condition for the survival of dust in the photospheric environment is that it is destroyed before it will grow too large. Then, the notion of dust formation may be somewhat different in the photospheric environment from that in circumstellar and interstellar cases. We conclude that only small grains that failed to be the stable large grains can be sustained in the static photosphere and will play an important role in determining the photospheric structure.

4.2. Unified Model Photospheres with the Dust Cloud

We now consider the photosphere in which the thermodynamical condition of condensation is fulfilled. We assume that dust forms as soon as temperature is lower than the condensation temperature (T_{cond}), but the dust will soon grow larger than its critical radius r_{cr} at the slightly lower temperature, say T_{cr} , which we referred to as the critical temperature. Thus, in the region with $T < T_{\text{cr}}$ in the photosphere, dust will be large enough and may segregate from the gaseous mixture. Since it is difficult to sustain such large dust grains in the photosphere, they eventually precipitate below the photosphere where they may evaporate. Only in the region with $T_{\text{cr}} \lesssim T \lesssim T_{\text{cond}}$, the dust grains will be small enough ($r_{\text{gr}} \lesssim r_{\text{cr}}$) to be sustained in the photosphere and it is such small dust grains that play an important role as opacity sources. Thus, the dust effectively exists only in the restricted region located relatively

deep in the photosphere, and this means that a dust layer (or a cloud) is formed in the photosphere. Thus, the cloud formation is a natural consequence of considering not only dust formation but also its segregation.

Now, a major problem is to find the temperatures that define the dust cloud. The condensation temperature T_{cond} is easily found from the thermochemical computation to be $T_{\text{cond}} \approx 2000$ K for corundum and iron, which first form in the photospheres of ultracool dwarfs (as for detail, see Figs. 2-4). On the other hand, the critical temperature T_{cr} is more difficult to find. This should in principle be determined from the detailed analysis of the dust-gas segregation process, but it still seems to be premature to solve this problem theoretically. Instead, we treat T_{cr} as a free parameter to be found empirically. Since T_{cr} essentially determines the thickness of the dust cloud, which in turn should give significant effect on observables, T_{cr} could in principle be determined from observations.

So far, we have not yet specified the critical radius r_{cr} whose exact value is difficult to know, since it depends on the detail of the nucleation process. However, the minimum value of astronomical grains known in the literature is about $0.01\mu\text{m}$, and this may imply that the grains of about this size are already well stabilized. Then, we assumed that the critical size r_{cr} below which the grains are unstable and in detailed balance with the gaseous mixture is about $0.01\mu\text{m}$ (10 nanometer) or smaller. Then, the mass absorption coefficient of such dust grains, whose radii are sufficiently smaller than the wavelengths of interest, is almost independent of the grain size distribution (Sect.3.3), and our models are almost independent of the size distribution of dust grains under this assumption.

It is to be noted that the dust cloud can be found in all the cool dwarfs with $T_{\text{eff}} \lesssim 2600$ K. For objects with very low T_{eff} near 1000 K, the dust cloud formed near the dust condensation temperature ($T_{\text{cond}} \approx 2000$ K) may be situated too deep in the photosphere (where $\tau_{\text{Ross}} > 1$, since $T \approx T_{\text{eff}}$ at $\tau_{\text{Ross}} \approx 1$), while the dust cloud may appear in the optically thin region of the photosphere for relatively warm objects. This may explain why L dwarfs appear to be dusty while cooler T dwarfs show little evidence for dust. Thus our cloudy models will provide unified explanation on the dusty L dwarfs and apparently dust-free T dwarfs by a single sequence of model photospheres.

Finally, our initial attempts considered three different cases referred to as cases A (dust-free model), B (dusty model) and C (dust-segregated model) which correspond to $r_{\text{gr}} = 0$, $r_{\text{gr}} < r_{\text{cr}}$ and $r_{\text{gr}} \gtrsim r_{\text{cr}}$, respectively, and model photospheres were constructed based on the assumption that each case prevails throughout the photosphere (Tsuji 2000). However, it is difficult to explain why different cases should apply to different objects, while this difficulty is relaxed in our unified models. In fact, such idealized cases will never be realized in nature and the resulting models may be of little practical use for now (Sect. 7). But they represent the extreme limiting cases of our unified cloudy models: The dusty model of case B assumed that dust formed at $T = T_{\text{cond}}$ fills in the photosphere up to the surface, and thus represents a special extreme case of $T_{\text{cr}} = T_0$ where T_0 is the surface temperature. Also, the dust-segregated model of case C implies that the dust grains formed at $T = T_{\text{cond}}$ segregate as soon as they are formed, and this is another extreme case of $T_{\text{cr}} = T_{\text{cond}}$.

4.3. Non-Grey Radiative-Convective Model Photospheres

With the dust cloud outlined in the previous section, model photospheres based on the usual assumptions of hydrostatic and radiative equilibria are constructed. We assume LTE throughout. Also, plane parallel geometry can safely be assumed for the photospheres of cool dwarfs. From the viewpoint

of modeling the photosphere, the dust cloud simply introduces a large increase of opacities at some layer in the photosphere, and nothing is changed from the usual modeling of stellar photosphere, even though numerical computations are somewhat more complicated.

In the integration of model photosphere, we used the optical depth defined by the continuous opacity at $0.81\mu\text{m}$ and this independent variable is referred to as τ_0 . The step of integration is either $\Delta \log \tau_0 = 0.1$ ($T_{\text{eff}} > 1400\text{ K}$) or 0.05 ($T_{\text{eff}} \lesssim 1400\text{ K}$) for $\log \tau_0$ between -7.0 and 1.9. We divided the spectral region between $0.25\mu\text{m}$ and $50\mu\text{m}$ into 201 meshes during iterations. We generally approximated the line opacities by a three-step ODF in each spectral mesh, and thus any quantity related to the radiation field is evaluated at 201×3 frequency points. The final iteration, however, is done with 665 meshes (again with a three-step ODF).

As is well known, convective energy transport is efficient at high densities of compact objects. We first constructed pure radiative equilibrium model by our iterative temperature correction procedures. Then, if the model is found to be convectively unstable, we have applied the local mixing length theory (LMLT) to take into account the effect of convection. Then, we examine if the model satisfies

$$\pi F_{\text{rad}}(\tau_0) + \pi F_{\text{conv}}(\tau_0) = \sigma T_{\text{eff}}^4, \quad (7)$$

where $F_{\text{rad}}(\tau_0)$ is evaluated by solving the transfer equation and $F_{\text{conv}}(\tau_0)$ is the convective flux given by the LMLT. If the model does not satisfy eqn.(7), we again applied the iterative temperature correction procedures. It is required, however, that the radiative flux should be $F_{\text{rad}}(\tau_0) = \sigma T_{\text{eff}}^4/\pi - F_{\text{conv}}(\tau_0)$ rather than $\sigma T_{\text{eff}}^4/\pi$. For the iterated model, the LMLT is again applied to evaluate convective flux, and these processes are repeated until convergence is obtained.

Here, however, at the onset of convection in the optically thin photosphere, say $\tau_0 \approx 0.01$, the convective flux of a few % of the total flux appears suddenly, but it is difficult for radiative flux to decrease by the same amount suddenly because of the non-local character of the radiative flux. Thus it is difficult to satisfy eqn.(7) by better than a few % at the interface of the radiative and convective zones in some cases. This problem is related to the inherent difficulty of the present LMLT, which is essentially a local theory but coupled with the non-local theory of radiative transfer. Probably, the flux error at the radiative-convective interface can be resolved by considering the overshooting of the convective cells to the radiative zone, and it may be of little meaning to try to reduce the flux error of a few % within the framework of the LMLT.

5. PHYSICAL STRUCTURE OF THE UNIFIED CLOUDY MODELS

We now apply the method of the non-grey model photosphere to the ultracool dwarfs with the dust cloud deep in the photosphere. The basic input parameters that specify a classical model photosphere are chemical composition, effective temperature, surface gravity and micro-turbulent velocity. If dust forms in the photosphere, however, we have to introduce an additional parameter, the critical temperature T_{cr} , and we examine its effect by assuming four cases of $T_{\text{cr}} = 1600, 1700, 1800$ and 1900 K in addition to the extreme limiting cases of $T_{\text{cr}} = T_0$ (case B) and $T_{\text{cr}} = T_{\text{cond}}$ (case C) (Sect.5.1). The chemical composition can be arbitrary changed but we restricted to the case of the solar system mixture discussed in Sect.2.1 in this paper. We also assumed $\log g = 5.0$ throughout and the micro-turbulent velocity in the photosphere is assumed to be 1.0 km sec^{-1} , which is near the solar value. We have computed grids of model photospheres for the six values of T_{cr} noted above (Sect.5.2). The presence of dust cloud results in a significant effect on the convective structure of cool dwarfs (Sect.5.3).

5.1. Effect of the Critical Temperature

We first examine the effect of the critical temperature T_{cr} on the thermal structure of the photosphere, and discuss its effect in some detail for the case of $T_{\text{eff}} = 1800 \text{ K}$ as an example. The resulting thermal structures are shown in the top panel of Fig.2a for six values of T_{cr} , namely T_0 (case B), 1600, 1700, 1800, 1900, and T_{cond} (case C). The lower boundary of the dust cloud is defined by the condensation line of corundum (Al_2O_3) or of iron (Fe) shown by the dot-dashed line in Fig.2a and the upper boundary by T_{cr} indicated by the plus sign for each model. Thus, the value of T_{cr} essentially specifies the thickness of the dust cloud. In Fig.2a, the resulting structures of our cloudy models are found between the dusty (cases B) and dust-segregated (case C) models as expected.

The thermal structure of the case B model (i.e. $T_{\text{cr}} = T_0$) is rather peculiar in that it nearly coincides with the iron condensation line in the surface region. This is a general characteristic of the case B models whose photosphere is fully filled in by dust (see further Fig. 4) and this is because iron works as a thermostat: If iron grains are formed, they effectively absorb radiation and the temperature of the iron forming region rises. Then the iron grains may evaporate and the temperature drops. Then, iron grains may form again and so on. Thus, temperatures remain relatively high in the case B model throughout the photosphere. In another extreme model of case C ($T_{\text{cr}} = T_{\text{cond}}$), the surface temperature is very low ($T_0 \approx 800 \text{ K}$ for $T_{\text{eff}} = 1800 \text{ K}$). This is due to the cooling effect of the highly non-grey opacities of the volatile molecules that are abundant in this case but no heating due to dust.

The formation of the dust cloud ($T_{\text{cr}} \lesssim T \lesssim T_{\text{cond}}$, where $T_{\text{cr}} = 1600, 1700, 1800$ and 1900 K with $T_{\text{cond}} \approx 2000 \text{ K}$) results in a drastic change of the thermal structure against the case of fully dusty model of case B. Here, the role of iron as thermostat can still be seen in the cases of $T_{\text{cr}} = 1600$ and 1700 K , but it no longer plays a significant role in the cases of $T_{\text{cr}} = 1800$ and 1900 K possibly because the amount of iron grains may not be large enough for this effect to work. On the other hand, dust has precipitated in the surface region above the dust cloud (where $T < T_{\text{cr}}$) and volatile molecules dominate there. The photosphere is cooled appreciably by the cooling effect of the infrared molecular bands of the volatile molecules as in our case C model. The thermal structure of the upper photosphere is determined by the balance of the heating due to dust grains in the cloud and the cooling by the molecules above the cloud. The temperatures in the surface region are lower for the higher T_{cr} , since the mass column density of the volatile molecules above the dust cloud should be larger. The photospheric structures of the cloudy models approach to that of the case B model in the region below the dust cloud (where $T > T_{\text{cond}}$).

In the case of $T_{\text{eff}} = 1400 \text{ K}$ shown in Fig.2b, the thermal structure of the case B model coincides with the iron condensation line only partly and shows considerable cooling in the surface region either by the infrared bands of silicate or by the molecules coexisting with the dust grains. The formation of the dust cloud results in a more drastic change of the thermal structure against the case of fully dusty model of case B than in the case of $T_{\text{eff}} = 1800 \text{ K}$ (Fig.2a). Here, the sudden increase of opacity due to the formation of dust cloud at $T = T_{\text{cr}}$ results in very steep temperature gradient and, for this reason, temperature shows steep upturn, which starts at the shallower layer for the smaller T_{cr} . The photospheric structure of the cloudy model again approaches to that of the case B model in the region below the dust cloud (where $T > T_{\text{cond}}$). On the other hand, dust-free region above the dust cloud (where $T < T_{\text{cr}}$) is more extended and the cooling effect due to the infrared molecular bands of the volatile molecules is more effective than in the case of $T_{\text{eff}} = 1800 \text{ K}$ (Fig.2a). For this reason, the thermal structures of the cloudy models approach to that of the case C model in the surface region.

The case of the lower T_{eff} near 1000 K , the effects of the dust cloud on the thermal structure are

essentially the same as in the case of $T_{\text{eff}} = 1400 \text{ K}$, except that its effect is less important on the structure of the surface region. For this reason, the structure of the cloudy model approaches to that of the case C in the upper photosphere, and to the case B model in the deeper region of the photosphere. A preliminary version of the cloudy model for the case of $T_{\text{eff}} = 1000 \text{ K}$ with $T_{\text{cr}} = 1550 \text{ K}$ was discussed before (Tsuji et al. 1999).

In general, iron (Fe) and corundum (Al_2O_3) condense at their condensation lines before the cloud forming region terminates at $T \approx T_{\text{cr}}$. However, enstatite (MgSiO_3) is outside the cloud zone and this means that enstatite has segregated as soon as it is formed within the framework of our simplified treatment of the dust cloud. This may be possible because enstatite will easily form with corundum and/or iron as the seed nucleus and grow rapidly. For the same reason, other solid species that may form at the lower temperatures will precipitate as soon as they are formed. For this reason, only the dust species formed at relatively high temperatures above T_{cr} work as the active dust (i.e. as sources of opacity) and hence give significant effect on the photospheric structure. This fact may simplify the construction of the cloudy models since it is enough to consider only a few high temperature condensates such as corundum and iron as sources of opacity. In some cases (e.g. $T_{\text{eff}} = 1400 \text{ K}$ with $T_{\text{cr}} = 1600 \text{ K}$), however, a small amount of enstatite may form in the upper part of the dust cloud.

5.2. Grids of the Unified Cloudy Models

As shown in the previous subsection, the photospheric structure under the presence of the dust depends on a new parameter which we referred to as the critical temperature T_{cr} . We have computed grids of model photospheres with $T_{\text{cr}} = 1600, 1700, 1800$ and 1900 K for the effective temperature range between 800 and 2600 K . These grids are to be used to predict observables and to determine T_{cr} by consulting with observed data (e.g. Sect.7.1). As an example, we discuss the case of $T_{\text{cr}} = 1800 \text{ K}$ and the resulting models are shown in Fig.3, where the cloud zone is shown by the dotted area.

In Fig.3, the locus of the Rosseland mean optical depth (τ_R) unity is shown by the dashed line. The locus of $\tau_R \approx 1$ roughly corresponds to $T \approx T_{\text{eff}}$ but not exactly because of the large non-grayness of the opacity. Nevertheless, it is interesting to note that the dust cloud is situated in the regimes of $\tau_R > 1$, $\tau_R \approx 1$, and $\tau_R < 1$ for the models of $T_{\text{eff}} \lesssim 1300$, $T_{\text{eff}} \approx 1400 - 1600$, and $T_{\text{eff}} \gtrsim 1700 \text{ K}$, respectively. This result indicates that the dust cloud should be situated within the optically thin regime in the relatively warm objects with $T_{\text{eff}} \gtrsim 1700 \text{ K}$, and this fact provides a natural explanation why L dwarfs appear to be dusty. On the other hand, the dust cloud should be situated within the optically thick regime in the relatively cold objects with $T_{\text{eff}} \lesssim 1300 \text{ K}$, and this fact explains why T dwarfs apparently show little evidence for dust. The cloud may be situated near the optical depth unity in the objects with $T_{\text{eff}} \approx 1400 - 1600 \text{ K}$, which may just explain the early T dwarfs or L/T transition objects recently discovered by Leggett et al. (2000).

Finally, instead of presenting the grids for other T_{cr} 's, we show the grids for the extreme limiting cases B and C by the dashed and dotted lines, respectively, in Fig.4. It is to be noted that all the case B models with $T_{\text{eff}} \gtrsim 1800 \text{ K}$ converges to the iron condensation line. All the cloudy models of a given T_{eff} can be found between the models of cases B and C of the same T_{eff} as shown in Fig. 2. Also all the cloudy models as well as those by the cases B and C of a given T_{eff} degenerate to a single model for $T_{\text{eff}} > 2600 \text{ K}$, in which dust no longer plays a major role. Then, our case C models represent the models of $T_{\text{eff}} > 2600 \text{ K}$ and extended to $T_{\text{eff}} = 4000 \text{ K}$ as shown by the solid lines in Fig.4. It is noted

that the models of $T_{\text{eff}} = 2800 - 3200$ K cross the dust condensation lines, but a small amount of dust grains formed in the very surface of the photosphere gives little effect on the physical properties of the models.

5.3. Convection

In the lower six panels of Figs.2a & 2b, convective, radiative, and total fluxes normalized by $\sigma T_{\text{eff}}^4 / \pi$ are shown with the dashed, dotted, and solid lines, respectively, for the six values of T_{cr} . In the case of $T_{\text{eff}} = 1800$ K (Fig.2a), the photosphere approaches to the wholly convective in the deepest region in all the cases, and the structure of the convective zone is rather simple. The cloudy models as well as the dusty model of case B show essentially the same convective structure as the case C model and the dust cloud gives little effect on the convective structure. This may be because the dust cloud is situated in the optically thin regime in the photosphere and the amount of dust is not yet very large.

The situation is quite different in the case of $T_{\text{eff}} = 1400$ K (Fig.2b), in which the dust cloud is formed deep in the photosphere: The temperature gradient is quite steep near the dust cloud because of the high opacity due to the dust and the model is convectively unstable near T_{cr} . For this reason, our cloudy models show the outer convective zone in addition to the one in the inner deep region. This new convective zone is separated by an intermediate or detached radiative zone in all our cloudy models, as discussed in the case of the hybrid model of $T_{\text{eff}} = 1000$ K with $T_{\text{cr}} = 1550$ K applied to Gl 229B (Tsui et al. 1999). It is to be noted that such an outer convective zone does not appear in our case B model despite the large dust opacity. This may be because of the rather modest temperature gradient due to the heating effect of dust, and the large opacity does not necessarily induce convection.

In Fig.5a, some detail of the convective zone of the cloudy models with $T_{\text{cr}} = 1800$ K (Fig.3) are shown for T_{eff} between 800 and 2600 K with a step of 200 K. In the models of $T_{\text{eff}} \gtrsim 1800$ K, the dust cloud does not induce convection as also noted on Fig.2a. In the model of $T_{\text{eff}} = 1600$ K, the outer convective zone separated from the inner convective zone appears, but the convective flux is rather small. The outer convective zone develops further as the dust cloud moves to the inner dense region in the models with $T_{\text{eff}} \lesssim 1400$ K. The outer convective zone, however, merges with the inner convective zone in the models with $T_{\text{eff}} \lesssim 1000$ K.

The convective velocities of the same models discussed above are shown in Fig.5b and appear to be rather small in general. For example, $V_{\text{conv}} \approx 80$ m sec $^{-1}$ in the hottest model and as small as 10 m sec $^{-1}$ in the coolest model. This is a natural consequence that only small convective velocity is sufficient to transport the given energy flux under the very high densities of the photospheres of ultracool dwarfs. Although the mixing length is assumed to be one pressure scale height throughout, the super-adiabaticity is very small and the results depend little on the mixing length.

It is to be remembered that our models are based on the local mixing length theory (LMLT) and it is within the framework of the LMLT that a thin outer convective zone is predicted. However, it is unknown if the rather thin convective zone can be stable or if it may induce some dynamical effects. We defer more detailed analysis of the complicated structure of the convective zone in the cloudy model to future works, but the presence of the convectively unstable regime beside the one in the deeper region is a characteristic feature of the cloudy model of ultracool dwarfs.

Even within the framework of the LMLT, however, it was rather difficult to achieve the flux con-

stancy within 1% as is usually realized in non-grey model photospheres without dust. As shown in Fig.2 (also see Fig.5a), we had to allow flux errors of a few % especially at the edges of the outer convective zone. This should be due to essential difficulty to match the convective flux determined locally and the radiative flux of the non-local character (Sect.4.3). Also, appearance of the dust cloud at $T \approx T_{\text{cr}}$ results in a sudden increase of opacity and the requirement of the flux constancy had to be relaxed somewhat.

6. PREDICTED EMERGENT SPECTRA

Generally, stellar spectra could be interpreted in terms of effective temperature T_{eff} , surface gravity g , chemical composition, and micro-turbulent velocity. In ultracool dwarfs in which dust necessarily forms a cloud, at least one additional parameter that specifies the nature of the cloud should be necessary and we represented it by the critical temperature T_{cr} . After a brief survey on the spectroscopic data (Sect.6.1), we examine the effect of T_{cr} (Sect.6.2) and T_{eff} (Sect.6.3) on the emergent spectra, while other three parameters remain the same as noted in Sect.5.

6.1. Spectroscopic Data and Spectral Synthesis

Once a model photosphere is at hand, the emergent spectra can readily be computed for the given spectroscopic data. Unfortunately, however, available spectroscopic data are far from satisfactory and this is a major obstacle in predicting emergent spectra from model photospheres of ultracool dwarfs. As an example, we discuss the near infrared region for which spectroscopic as well observational data are relatively abundant.

We have prepared a spectroscopic database for the near infrared molecular lines including ^{12}CO , ^{13}CO , C^{17}O (Guelachivili et al. 1983; Chackerian & Tipping 1983), CN (Cerny et al. 1978; Bauschlicher, Langhoff, & Taylor 1998), OH (GEISA; Jacquinot-Husson et al. 1999), ^{28}SiO , ^{29}SiO , ^{30}SiO (Lavas, Maki, & Olson 1981; Tipping & Chackerian 1981; Langhoff & Bauschlicher 1993), and H_2O (HITEMP; Rothman 1997). We have also tried other H_2O data such as by Partridge & Schwenke (1997) and found that the differences with the HITEMP data are rather minor (typically, $\Delta \log gf < 0.1$ and $\Delta \omega < 0.1 \text{ cm}^{-1}$).

For other molecules including CH_4 , NH_3 , PH_3 , and H_2S , however, available linelists are limited to the low excitation lines of some restricted bands and are far short for our purpose. We regard the effect of these polyatomics as pseudo-continua and apply the band model method to evaluate the absorption coefficients (Sect.3.1). The electronic bands such as of FeH, TiO, and VO have some effects near $1 \mu\text{m}$, and we also treated them as pseudo-continua. Also a few lines of K I (Wiese, Smith, & Miles 1969) are added but we do not intend to include comprehensive lilelists of atomic lines at present.

The spectra were calculated with an interval of $0.05 - 0.1 \text{ cm}^{-1}$ and then convolved with the slit function which is assumed to be the Gaussian with FWHM typically 500 km sec^{-1} ($R = 600$). The computation of the spectra for the cloudy models can be done with any spectral synthesis code by simply adding the dust absorption and scattering coefficients to the continuous absorption and scattering coefficients, respectively, in the temperature range of $T_{\text{cr}} \lesssim T \lesssim T_{\text{cond}}$.

6.2. Effect of the Critical Temperature

The effect of the dust cloud on the emergent spectra may be twofold: One is the direct effect due to the extinction by the dust opacities and the other is the indirect effect due to the change of the structure by the dust cloud. Also, since dust appears in the form of cloud, not only the thickness of the cloud but also its location as seen against optical depth changes even though the dust cloud always form at the same temperature range of $T_{\text{cr}} \lesssim T \lesssim T_{\text{cond}}$. The spectra reflect all these effects.

The predicted spectra between 1 and 4 μm based on the models of $T_{\text{eff}} = 1800\text{ K}$ are shown for $T_{\text{cr}} = 1600, 1700, 1800$, and 1900 K as well as for cases B and C in Fig.6a. In these models of $T_{\text{eff}} = 1800\text{ K}$, the dust cloud is in the optically thin regime and the cloud itself may be still optically thin. Yet the dust cloud produces considerable extinction in the J band region. Especially, the dust cloud produces noticeable extinction in the case of $T_{\text{cr}} = 1600\text{ K}$, in which the spectrum is indistinguishable from that of case B. The strong H_2O 2.7 μm bands, which are sensitive to the thermal structure of the surface region, appear to be stronger for the higher T_{cr} for which the temperatures in the surface region are lower (Fig. 2a). It is interesting to see in Fig.6a that the P and R branches as well as the strong Q branch of the $\text{CH}_4 \nu_3$ bands appears already at $T_{\text{eff}} = 1800\text{ K}$ in the case of $T_{\text{cr}} = 1800\text{ K}$ and strengthens towards higher T_{cr} (only Q branch appears in the case of $T_{\text{cr}} = 1700\text{ K}$).

In the case of $T_{\text{eff}} = 1400\text{ K}$ shown in Fig.6b, the predicted spectrum of case B is close to the black-body radiation of $T \approx 1400\text{ K}$, and this implies that the observable photosphere filled in by dust is now optically thick. Also, the difference of the spectra for case B and for the cloudy models is quite large. This is because the dust grains in the region of $T < T_{\text{cr}}$ have precipitated in the cloudy models and the dust extinction has decreased drastically. The optical thickness of the cloud in the observable photosphere is smaller for the higher T_{cr} , and the extinction in the J band region should decrease. At the same time, the column densities of volatile molecules above the cloud increase for the higher T_{cr} as the upper boundary of the dust cloud moves to the deeper layer and the molecular bands such as of H_2O and CH_4 strengthen.

Finally, in the case of $T_{\text{eff}} = 1000\text{ K}$ shown in Fig.6c, the predicted spectrum of case B shows weakly the Q branch of the $\text{CH}_4 \nu_3$ bands, despite the large extinction by the dust. On the other hand, the cloudy models show very strong bands of volatile molecules such as of H_2O and CH_4 , but the effect of dust is rather minor for any value of T_{cr} . This is because the dust cloud is now situated very deep in the photosphere below the observable layer and volatile molecules dominate almost the entire region of the observable photosphere above the cloud. This result implies that the presence of dust cloud deep in the photosphere gives little effect on the emergent spectra for very cool T dwarfs with $T_{\text{eff}} \lesssim 1000\text{ K}$. This fact implies that rather simple dust-segregated models (case C) can be used for discussing observed spectra of cool T dwarfs, even though the dust deep in the photosphere gives considerable effect on the structure of the inner photosphere.

6.3. Dependence on the Effective Temperature

We show the effect of T_{eff} on the emergent spectra between 1 and 2.6 μm based on our unified cloudy models with $T_{\text{cr}} = 1800\text{ K}$ in Fig.7 (we showed the spectra by a step of 200 K in T_{eff} to avoid confusion although computations are done by a step of 100 K). We also included the models of $T_{\text{eff}} > 2600\text{ K}$ in which dust no longer plays a major role and, for this purpose, we apply our grid of the case C models.

Thus, Fig.7 will give some idea on the change of the infrared spectra through M, L, and T dwarfs. We indicated T_{eff} in units of 100 K on some spectra, and some spectral features are identified.

For $T_{\text{eff}} > 2600$ K, there is no effect of dust, and dust extinction is still almost negligible at $T_{\text{eff}} \approx 2600$ K even if a small amount of dust is formed ($T_{\text{cr}} < 1800$ K). The effect of the dust extinction gradually increases at the J band region for the models with $T_{\text{eff}} < 2600$ K so long as the dust cloud is located within the optically thin regime. This effect is the largest at $T_{\text{eff}} \approx 1600$ K, where molecular bands appear to be dimmed seriously. We confirmed that the spectra degenerate into almost the same one for the models of $T_{\text{eff}} = 1500, 1600$, and 1700 K at the J band region, although this degeneracy disappears in the H and K band regions. This may be because the dust cloud now penetrates into the optically thick regime while the dust column density of the cloud itself may also increase as the cloud moves to deeper (and hence denser) region. Because of these two effects, the dust column density in the observable photosphere may remain nearly the same for $1500 \lesssim T_{\text{eff}} \lesssim 1700$ K. Finally, the dust extinction begins to decreases in $T_{\text{eff}} \lesssim 1400$ K according as the dust cloud moves to the deeper photosphere. At the same time, abundances of the volatile molecules in the region above the cloud increase, and the molecular bands strengthen rapidly towards cooler models.

The water bands are visible at $T_{\text{eff}} \approx 3000$ K or higher and and strengthen towards the lower T_{eff} 's. However, increase of the water bands is rather modest in $1600 < T_{\text{eff}} < 2000$ K, and this may be because the increased H_2O abundance with decreasing T_{eff} is compensated for by the increased dust extinction. In $T_{\text{eff}} \lesssim 1400$ K, the increasing H_2O abundance and deceasing dust in the observable photosphere with decreasing T_{eff} result in a rapid strengthening of the H_2O bands. The CH_4 $2.2\mu\text{m}$ bands appear at $T_{\text{eff}} \approx 1600$ K by the low resolution ($R = 600$) employed in this figure while those at $1.6\mu\text{m}$ bands appear at $T_{\text{eff}} \approx 1500$ K. At the same time, the CO $2.3\mu\text{m}$ bands, which are already prominent at $T_{\text{eff}} \approx 4000$ K, almost disappear at $T_{\text{eff}} < 1400$ K. As we noted in Sect.6.2, not only the Q branch but also the P and R branches of the stronger CH_4 $3.3\mu\text{m}$ bands appear already at $T_{\text{eff}} = 1800$ K for the cloudy models with $T_{\text{cr}} = 1800$ K or higher.

7. COMPARISONS WITH OBSERVATIONS

The emergent spectra of our cloudy models show characteristic changes with T_{cr} (Fig.6) as well with T_{eff} (Fig.7). Such characteristics can most simply be represented by the infrared colors, which in turn can be compared with observations. It is shown that the effects of T_{cr} and T_{eff} on the infrared colors can be separated and this fact makes it possible to estimate T_{cr} from the infrared colors (Sect.8.1). The observed spectral features of ultracool dwarfs can directly be compared with the predicted ones based on our models (Sect.8.2). Also, some detail of water and methane bands will be discussed as a preliminary step towards detailed quantitative analyses of the spectra of ultracool dwarfs (Sect.8.3).

7.1. Infrared Colors and Estimation of T_{cr} and T_{eff}

Infrared photometry in the J , H , and K (or K_s) bands has extensively been applied to ultracool dwarfs including L and T dwarfs. As examples, we show observed infrared colors $J - K$, $J - H$, and $H - K$ on the Mauna Kea Observatories (MKO) system (Leggett et al. 2002) against the spectral types defined by Geballe et al. (2002) in Fig.8a. An interesting feature is that all these infrared colors are not necessarily redder for the later types but show the red limit at about L5 - 6, as first noted by Kirkpatrick

et al. (1999).

Based on the emergent spectra discussed in Sect.6, we tried to predict the infrared colors on the J, H, K photometry. We apply the filter response function for the MKO system (Simon & Tokunaga 2002; Tokunaga, Simon, & Vacca 2002) and then the resulting colors are converted to the same scale as the observed colors by using the model spectrum of Vega (Kurucz 1994). The resulting predicted colors based on our grids of the models with $T_{\text{cr}} = 1600, 1700, 1800$, and 1900 K as well as of our cases B and C models are shown in Fig.8b for comparison with observations.

It is to be noted that all our cloudy models predict the presence of the red limits at about $T_{\text{eff}} \approx 1600$ K while our cases B and C fail to do. Thus, Fig.8 can be regarded as a clear demonstration that only the cloudy models are realistic enough in explaining the observed infrared colors. It is to be noted that the case B models predict much redder colors for cooler models while our case C models never predict such red colors as observed for any value of T_{eff} . This later result clearly demonstrates that the reddening of the infrared colors in late M and L dwarfs is not due to the line blanketing effect of molecular bands but should mostly be due to the effect of the dust.

The presence of the red limits in the infrared colors should be a natural consequence of the presence of a dust cloud deep in the photosphere. For a given value of T_{cr} , the thickness of the cloud always corresponds to $T_{\text{cond}} - T_{\text{cr}}$ if seen by temperature and the cloud is situated at the same temperature range of $T_{\text{cr}} \lesssim T \lesssim T_{\text{cond}}$, but the dust column density of the cloud increases for cooler T_{eff} , since the cloud is situated in the inner (and hence denser) region if seen by the optical depth. Thus, so far as the dust cloud is located in the optically thin region, as is the case for models with $T_{\text{eff}} \gtrsim 1600$ K (Fig.3), the infrared colors will be redder for cooler models because of the increased dust extinction due to the increased dust column density. On the other hand, once the dust cloud penetrates into the optically thick region in models with $T_{\text{eff}} \lesssim 1500$ K (Fig.3), the dust column density in the observable photosphere decreases and, at the same time, the column density of the molecular gas above the cloud increases. For this reason, the infrared colors turn to blueward until they finally merge with the infrared colors of the case C models at the coolest model (Fig.8b).

The results in Fig.8b show that the infrared colors are redder for the lower value of T_{cr} at a given T_{eff} , and this is because the thickness of the dust cloud is larger for the lower value of T_{cr} at any given T_{eff} . Then, it is in principle possible to estimate T_{cr} by a comparison of the observed (Fig.8a) and predicted (Fig.8b) colors. So far, we have assumed the same value of T_{cr} for the range of $800 \lesssim T_{\text{eff}} \lesssim 2600$ K, but this should most probably be unrealistic. For simplicity, however, we assume that late L dwarfs can be represented by the models of the same T_{cr} . Since the effect of the dust cloud on observables is more prominent in L dwarfs than in T dwarfs, we are primarily interested in the nature of the cloud in L dwarfs. Then, we estimated that the maxima of the mean values of the observed $J - K, J - H$, and $H - K$, are about 1.8, 1.0, and 0.8, respectively, at about L5.5 (Fig.8a), and these maxima can roughly be reproduced at about $T_{\text{eff}} = 1600$ K by the predicted $J - K, J - H$, and $H - K$ with $T_{\text{cr}} = 1800$ or slightly lower (Fig.8b). From this result, we suggest that T_{cr} should be close to 1800 K and we apply $T_{\text{cr}} = 1800$ K in the rest of this paper. This result implies that the dust cloud may be rather thin at least in late L dwarfs.

Also, our preliminary analysis on the different observed data based on the J, H , and K_s photometry (Kirkpatrick et al. 1999, 2000) arrived at the same conclusion of $T_{\text{cr}} = 1800$ K (Tsuji 2001). On the other hand, our previous suggestion of $T_{\text{cr}} = 1550$ K for a model of $T_{\text{eff}} = 1000$ K was largely biased by the analysis of the optical spectrum of Gl 229B (Tsuji et al. 1999). However, we now know that the dust cloud is situated too deep to give appreciable effect on the observed spectrum in the case of

such a cool T dwarf, and the estimation of T_{cr} should be difficult in such a case. With this difficulty in mind, the modest dependence of the emergent spectra on T_{cr} for the case of 1000 K (Fig.6c) can be used to constrain somewhat the value of T_{cr} and our revised analysis of the optical spectrum of Gl 229B appeared to be consistent with $T_{\text{cr}} = 1800$ K (Tsuiji 2001).

It is to be noted, however, that the scattering in the observed data are rather large and this fact may suggest that the thickness of the dust cloud is not necessarily the same even at a given T_{eff} . In fact, the scattering of the observed colors (Fig.8a) can be explained by the cloudy models of $T_{\text{cr}} \approx 1700 - 1850$ K (Fig.8b). As to the origin of the scattering, however, other effects such as of metallicity, age, mass, rotation, and other activities must also be considered. On the other hand, a safe conclusion is that the cases of $T_{\text{cr}} = 1600$ and 1900 K, which predicts the infrared colors too red and too blue, respectively, compared with the observed ones, may be excluded. Also, an encouraging result is that all the three predicted colors show the red limits at $T_{\text{eff}} \approx 1600$ K while the red limits of the three observed colors are all at about L5.5. This fact suggests that $T_{\text{eff}} \approx 1600$ K at about L5.5, and this result is almost free from the choice of T_{cr} .

Estimations of T_{eff} 's for other spectral types are more difficult. Colors are often used as indicators of stellar effective temperatures, but accurate calibration of color against T_{eff} is difficult for cool stars because of the severe line blanketing effect. As a preliminary attempt, we have estimated representative colors for several spectral types from a curve drawn by free-hand on each color-spectral type plot of Fig.8a. Then, T_{eff} is estimated for each color from Fig.8b, but the results depend on T_{cr} for which we assumed 1800 K for $J - K$, $J - H$ and $H - K$. The results are summarized in Table 2 and the mean T_{eff} from the three colors is also given for each subtype. The results from different colors are mostly within 100 K of the mean T_{eff} and thus internally consistent within about 100 K.

7.2. Spectral Indices

As an example of the spectral indices employed in the spectral classification, the H_2O 1.2 μm index defined by Geballe et al. (2002) is shown against their spectral type in Fig.9a. For comparison, we calculated this index on our predicted spectra (such as shown in Fig.7 but transformed to the F_{λ} scale) following the definition by Geballe et al. (2002) and the result is plotted on Fig.9b. The observed index shows rather modest increase in L dwarfs but shows steep increase in T dwarfs. On the other hand, the predicted index based on our cloudy models shows rapid upturn at $T_{\text{eff}} \approx 1400$ K which may correspond to the early T types in agreement with observations. The predicted index based on our case C models (dotted line in Fig.9b) shows upturn at about $T_{\text{eff}} \approx 1700$ K while that based on our case B models (dashed line) show no such rapid upturn in the T dwarf regime.

The observed CH_4 2.2 μm index by Geballe et al. (2002) is shown in Fig.10a while the predicted one based on our models in Fig.10b. The observed index shows that the methane 2.2 μm bands appear at early T types and our cloudy models predict that the bands appear at about $T_{\text{eff}} \approx 1500$ K in agreement with the results discussed in Sect.6.3. On the other hand, our case C models show that the CH_4 2.2 μm bands appear at $T_{\text{eff}} \approx 1700$ K. Also, our case B models show only weak methane bands in the T dwarf regime as expected.

As an example of atomic line features, the observed pseudo-EW's of K I 1.2432 μm given by Burgasser et al. (2002) are plotted against their spectral type in Fig.11a. For comparison, predicted EW's measured on the spectra based on our cloudy models (Fig. 7) are shown by the solid line while those

based on our cases B and C models by the dashed and dotted lines, respectively, in Fig.11b. The observed features show drop at late L types and our prediction based on the cloudy models also shows rapid decrease at $T_{\text{eff}} \approx 1500$ K, while this effect is not predicted by our case C models. The observed EW's again show upturn in the T dwarf regime, and this effect is also predicted by our cloudy models. Although the rapid decrease of the KI EW's in late L dwarfs can be explained by the case B models as well, the KI line totally disappears below about $T_{\text{eff}} \approx 1500$ K in the case B models. Thus the rather complicated behaviour of the KI line can be explained only by our cloudy models: The observed EW's of the KI line shows the minimum at about L7, and this is because the dust column density and hence the dust extinction are the largest at about $T_{\text{eff}} \approx 1600$ K in our cloudy models. According as the dust cloud moves to the inner region in the cooler models, the dust extinction decreases and the KI line strengthens again. The increase of the KI EW, however, cannot be so large in T dwarfs even if the dust column density in the observable photosphere decreases, because of the unfavourable excitation of the KI line at the low temperatures (1.2432 μm line originates from a level with 1.61 eV).

7.3. Water and Methane Bands

It is known that quantitative analyses of water bands showed serious difficulty in that predicted water bands appeared to be too strong compared with observations (e.g. Tinney, Mould, & Reid 1993). In fact, this problem was one of the motivations that we proposed the presence of dust in late M dwarfs (Tsuji et al. 1996a). Another possibility often mentioned is the incompleteness of the present linelists (e.g. Rothman 1997; Partridge & Schwenke 1997; Viti, Tennyson, & Polyansky 1997) which do not yet cover the high excited levels reasonably well. However, if the hot bands not yet included in the present linelist are added, predicted water bands will be stronger and the discrepancy with the observed ones may not be resolved.

Under such circumstances, we hoped that a solution can be provided by the recent revision of the solar oxygen abundance (Allende Prieto et al. 2001) noted in Sect.2.1, and we discuss this effect in some details for the case of the L dwarf prototype, GD 165B. For this $L3 \pm 1$ dwarf (Geballe et al. 2002), we may assume $T_{\text{eff}} \approx 1800$ K (Table 2). In Fig.12a, we compared the spectrum observed by Jones et al. (1994) with the predicted spectra based on the cloudy model ($T_{\text{eff}} = 1800$ K and $T_{\text{cr}} = 1800$ K) using the high oxygen abundance. The effect of silicate formation on H_2O abundance (Sect.2.3) is considered in the heavy solid line but not considered in the thin line. The two cases show little difference on the scale of Fig.12a and the reduction of H_2O abundance by 15 % (or -0.07 dex.) in the limited region of the photosphere gives only minor effect if oxygen abundance is sufficiently high compared with the carbon abundance. Also, it is to be noted in Fig.12a that the predicted water bands appear to be stronger as compared with the observed ones.

In Fig.12b, we compared the same observed spectrum with the predicted spectra based on the cloudy model ($T_{\text{eff}} = 1800$ K and $T_{\text{cr}} = 1800$ K) using the low oxygen abundance. The reduction of oxygen from the high abundance ($\log A_{\text{O}} = 8.91$) to the low abundance ($\log A_{\text{O}} = 8.69$) implies the reduction of $A_{\text{O}} - A_{\text{C}}$ and hence of the H_2O abundance by about a factor of 4 (with $\log A_{\text{C}} = 8.60$) so long as most carbon is in CO. For this reason, H_2O bands show rather large reduction for the decrease of oxygen abundance by a factor of 2, even for the case in which the effect of silicate formation on H_2O abundance is not considered (the thin solid line). Further, if the effect of silicate formation on H_2O abundance is considered, the reduction of H_2O abundance cannot be 15% but should be much larger, since the free gaseous oxygen is now very small (effectively equivalent to the case of $\log A_{\text{O}} =$

$\log A \approx 0.02$ or $A_O/A_C \approx 1.05$ as noted in Sect.2.3). The result shown by the heavy solid line clearly shows drastic effect of the silicate formation on H_2O abundance. Further, the CH_4 bands at $2.2\mu m$ are considerably enhanced.

Thus, we confirmed that the reduction of the free oxygen due to the silicate formation noted by Lodders & Fegley (2002) will give significant effect especially if the low solar oxygen abundance (Allende Prieto et al. 2001) is applied. However, this case is clearly not realistic, since water bands are too weak while methane bands are too strong compared with the observation. Nevertheless this fact alone may not be a reason to reject the low oxygen abundance, since what matters is the relative abundance of oxygen to carbon. In fact, if the solar oxygen abundance had to be revised by as much as a factor of 2, the solar abundances of carbon and nitrogen, which have been determined by more or less similar method as for oxygen, should also be reexamined. Until such a problem can be resolved, we cannot apply the new solar oxygen abundance to L and T dwarfs. For this reason, we discussed the models based on the high oxygen abundance (Table 1) throughout this paper.

In contrast to the case of water, major difficulty in discussing methane bands is the lack of spectroscopic data that can be applied to temperatures above the room temperature, even though there are some data in HITRAN (Rothman et al. 1998) and GEISA (Jacquinot-Husson et al. 1999). Hopefully, such excellent databases should not be restricted to investigating Earth’s atmosphere but be extended for applications to stellar and substellar problems. Without having other possibilities at present, we applied 56702 lines of $^{12}CH_4$ available in the GEISA database to evaluate synthetic spectra based on our model of $T_{eff} = 1000K$ with $T_{cr} = 1800K$, and the result is compared with the observed spectrum of Gl229B (Geballe et al. 1996; Oppenheimer et al. 1998; Leggett et al. 1999) in Fig.13a. It is clear that the predicted spectrum largely underestimates the strength of the observed methane bands, and this is what was expected since the linelist does not include many lines from the excited states. Even the ν_3 fundamental bands at $3.3\mu m$ could not be predicted well except possibly for the strong Q branch, and the situations with the 1.6 and $2.2\mu m$ bands are even worse.

Then, we apply the band model opacity (Sect.3.1) to methane bands in its simplest form, that is as a smeared-out pseudo-continuum (but we used the linelist for all the other molecules such as CO and H_2O). The resulting predicted spectrum is compared with the observed one in Fig.13b, and the agreement is now quite improved, especially for the 1.6 and $2.2\mu m$ bands. For this reason, we have used the band model opacity for methane throughout this paper, and we hope that the predicted methane bands based on this simple band model can be used for a while until a better linelist of methane can be available in the future. It is unfortunate, however, that the opacity had to be tested by the observed data of brown dwarf while what we should do is the reverse, even though the band model opacity of methane is tested by the linelist at least at the room temperature (Fig.14 in the Appendix).

8. DISCUSSION

8.1. Dust Cloud in the Photospheric Environment

A possibility that dust forms in stellar photosphere might have been conceived in the past but few attempts have been done to take the dust formation into account in modeling stellar photosphere. Probably, a drawback of including dust in modeling stellar photosphere may be because it was unknown how to treat dust in the photospheric condition. For example, it remained unknown how dust could be

sustained in the static photosphere. We propose a solution to this problem that the dust grains smaller than the critical size are in detailed balance with the surrounding gaseous mixture and hence can easily be sustained while grains larger than the critical size grow larger and may not be sustained in the static photosphere. The cloud formation is a natural consequence of the formation of dust at the condensation temperature T_{cond} and its segregation at the critical temperature T_{cr} , resulting in a dust cloud in the restricted region of $T_{\text{cr}} \lesssim T \lesssim T_{\text{cond}}$. Then, the classical non-gray theory of the stellar photosphere can directly be applied to the photosphere with a thin dust cloud and no other ad-hoc assumption is introduced at all to the classical theory of the stellar photosphere. Our basic assumption appears to be confirmed by the fact that the model photosphere based on this assumption predicts the observed spectra and colors reasonably well (Sect.7).

Our model is not yet complete in that the critical temperature cannot be determined from the physical theory but had to be treated as a free parameter to be determined empirically. Thus, our present model is semi-empirical in nature and we did not invoke the detail of the cloud formation mechanism. In this connection, an interesting attempt to determine the dust properties formed in the brown dwarfs was done by the analysis of the hydrodynamical processes induced by the acoustic wave originating in the convective zone (Helling et al. 2001). We hope that such an analysis will be developed to a fully *ab-initio* modeling including cloud formation.

Recently, formation of dust cloud has also been discussed by applying the method of planetary atmospheres (Ackerman & Marley 2001; Marley et al. 2002). Although we agree in that the dust cloud may be formed rather deep in the photosphere, there are some differences in detail. For example, they concluded that the grain sizes are as large as 10 - 100 μm while we assumed much smaller sizes below 0.01 μm . The observations of cool brown dwarfs such as Gl229B indicate that the large dust grains cannot be sustained in the observable photosphere. A question in the cloud model of Marley et al. (2002) is how such large grains can be sustained so nicely near the dust condensation temperature and why they do not fall further below that point. In our case, this problem is solved by considering only small grains that are in detailed balance with the gaseous mixture. Despite such a difference, the effect of the dust cloud on the thermal and convective structures was solved self-consistently both in their models and in ours. This has been a major issue in stellar model photosphere and this tradition is now extended to self-consistent models of substellar objects, in radiative-convective equilibrium under the presence of the dust cloud, by Marley et al.(2002) and by our present work. We agree further that one free parameter that specifies the thickness of the cloud had to be introduced; their f_{rain} and our T_{cr} . Thus, it appears that the cloud model based on the methodology of the planetary atmosphere is also semi-empirical in nature. This fact implies that it is still difficult to specify the nature of the cloud by the present theory of the planetary atmosphere as well as by that of the stellar photosphere.

8.2. Physical Basis of the Spectral Classification of L and T Dwarfs

We showed that a single grid of model photospheres with a thin dust cloud explains the major spectral features as well as the infrared colors of L and T dwarfs consistently. Although some spectral indices such as of water may also be accounted for by the dust-segregated models of case C (Sect.7.2), the infrared colors can never be explained by the case B nor by the case C models (Sect.7.1). This fact confirms that only the cloudy models provide the physical basis for the spectral classification of L and T dwarfs. Then, the systematic change of the colors and spectral features used in the spectral classification of L and T dwarfs can be interpreted as the effect of temperature and this fact confirms

that the proposed spectral classification of L and T dwarfs can be a reasonable one in that it represents a temperature sequence, even though the spectral classification has been done on purely empirical basis following the tradition since the classical Harvard system (Kirkpatrick et al. 1999, 2000; Geballe et al. 2002; Burgasser et al. 2002).

It is to be noted, however, that the major spectral indices used in the spectral classification of L and T dwarfs are not direct measures of stellar temperature as are usually the case in the spectral types from O to M, but are largely controlled by the presence of the dust cloud in the photosphere. At the same time, L and T types are not simply related to the amount of dust predicted by the chemical equilibrium theory while O - M types are directly connected to the abundances of atoms, ions, and molecules predicted by the ionization and dissociation theory. What is more important in L and T dwarfs is the location of the dust cloud in the photosphere: Since the dust cloud is always formed near the dust condensation temperature, its relative location in the photosphere moves from deep ($\tau > 1$) to surface ($\tau > 1$) regions according as T_{eff} increases from T to L dwarfs. It is this change of the location of the dust cloud that plays an important role in the characterization of the spectral types from L to T. Thus, although spectral types L and T can in principle be interpreted as a temperature sequence by the chemical thermodynamics, some non-equilibrium processes such as segregation, coagulation, and precipitation of dust grains must be considered. At present, the effects of these complicated processes are represented by the formation of the thin dust cloud deep in the photosphere, and this simple model explains the L - T spectral sequence quite well.

The spectral classification scheme of ultracool dwarfs, however, may not be deemed as well established yet. One problem is what is the major reason to discriminate L and T types. Probably, T type may be defined by the appearance of the methane bands, but it is now known that the CH_4 $3.3 \mu\text{m}$ bands appear at L5 (Noll, Geballe, & Marley 1997), and the 1.6 and/or $2.2 \mu\text{m}$ bands appear at late L dwarfs (Nakajima, Tsuji, & Yanagisawa 2001; McLean et al. 2001). Another problem is that the different L types show the same infrared color because of the red limit of the infrared colors at about L5-6. One possibility to resolve these inconveniences may be to terminate the L type at about the present L5-6 and to allocate T type to the later objects. This is in accord with the proposition by Geballe et al. (2002) to define T type by the appearance of the CH_4 $1.6 \mu\text{m}$ bands, and infrared colors can be unique for L types as well as for T types. This is, however, not proposing to change anything but for naming.

Although the L - T classification may represent a temperature sequence, accurate calibration of T_{eff} against the spectral type is not known yet. Our preliminary attempt (Sect.7.1) results in the Table 2, from which L dwarfs may start at about $T_{\text{eff}} \approx 2000 \text{ K}$ and may terminate at about $T_{\text{eff}} \approx 1450 \text{ K}$. Then, T dwarf sequence may start at about $T_{\text{eff}} \approx 1400 \text{ K}$ and extends to T_{eff} below 1000 K . We must remember, however, the limitation of the color method to estimate T_{eff} and an efficient method to relax this difficulty may be the infrared flux method (Blackwell, Petford, & Shallis 1980) which utilize the bolometric flux and an infrared flux that can be chosen to be relatively free from the severe line blanketing effect. Unfortunately, however, it is difficult to find such an infrared flux relatively free from the line blanketing effect in L and T dwarfs, even though it was still marginally possible in M dwarfs (Tsuji et al. 1996a). The most reliable method to estimate T_{eff} may be to measure bolometric flux of the ultracool dwarf with known parallax as noted by Burgasser et al. (2002). If T_{eff} can be determined on purely empirical basis, we hope that our result in Table 2 can be used for testing the models.

8.3. Observed Effects of Dust

It appears to be no doubt that the spectra and colors of late M dwarfs and L dwarfs suffer a considerable effect of dust extinction. These results may have two implications: First, dust formed in the photosphere of cool dwarfs should be well mixed with gas and uniformly cover the whole photosphere, since otherwise the effect of dust on spectra and colours cannot be so large as observed. Second, the dust in the photosphere of cool dwarfs will survive for a long time, as long as the Hubble time, since otherwise the dust could not be observed in so many cool dwarfs including the most late M dwarfs and L dwarfs. Our hypothesis that the dust grains formed in the photospheres of ultracool dwarfs should be very small ones which are in detailed balance with the gas will explain these results quite easily, since formation and destruction of such small grains will be repeating forever everywhere in the pohotosphere near the dust condensation temperature. On the other hand, it should be more difficult to consider a mechanism to sustain large dust grains for a long time in the static photosphere.

In a more detailed analysis of the spectra of dusty dwarfs, however, a difficult problem appears, that is an additional parameter which we referred to as the critical temerature had to be introduced. This parameter is essentially related to the thickness of the dust cloud or, more correctly, to the dust column density of the cloud in the observable photosphere. Unfortunately, direct determination of the dust column density in the observable photosphere is difficult, since dust shows no direct spectroscopic feature in the observed spectra. This is inherent difficulty in quantitative analyses of the spectra contaminated by dust and offers a formidarable problem. A more dificult case is the late T dwarfs in which the dust cloud may be situated too deep to give noticeable observable effect. The presence of the warm dust deep in the photosphere cannot be known directly by observations of the cool T dwarfs themselves, but can only be inferred from the results on the warmer objects in which the dust cloud appears in the optically thin regime. For this reason, it may not be possible to prove nor to disprove the presence of the warm dust deep in the photosphere by the analyses of the spectra of the coolest T dwarf such as SDSS 1624+00 (Nakajima et al. 2000; Liebert et al. 2000).

So far, we showed that T_{cr} can be inferred from the red limits of the infrared colors by assuming that T_{cr} may be the same at least for the reddest late L dwarfs (Sect.7.1). Although this assumption should most probably be too simplified, it may be difficult to determine T_{cr} for individual object. This is because colors (and any other observables) depend not only on T_{cr} but also on T_{eff} , and the effect of these two parameters could best be separated from the systematics on a large sample. Since T_{cond} is higher for the models of lower T_{eff} (Fig.3), T_{cr} may also be higher for the cooler dwarfs. We have prepared the model photospheres that may cover the possible range of T_{cr} and we hope that they can be used for estimating T_{cr} in ultracool dwarfs of different T_{eff} 's. For example, dust may be formed in late M dwarfs, but the dust cloud may be too thin for $T_{\text{cr}} \approx 1800$ K, since T_{cond} may already be close to 1800 K in late M dwarfs (Fig.3). Clearly, we cannot apply the same value of T_{cr} to M dwarfs as for L dwarfs, and we hope that some methods to estimate T_{cr} in M dwarfs can be developed.

Another problem related to dust is if it may induce some meteorological phenomena which may explain the unknown type of observed light variations in some ultracool dwarfs (e.g. Bailer-Jones & Mundt 2001; Martín, Zapatero Osorio, & Lehto 2001). Even if the dust cloud composed of the small grains is quite stable as noted above, it may be possible that some inhomogeneities develope in the cloud. Also, we do not yet consider the fate of the large grains which we assumed to have precipitated below the observable photosphere and might have evaporated there. It may be possible that the large grains do not necessarily precipitate so easily but remain in the photosphere as real “clouds” which are more familiar to us on the Earth. Such “clouds” should have only a small filling factor of the stellar surface,

since otherwise their effect should be observable in T dwarfs as well. We have not yet considered the fate of the large grains that have segregated from the gaseous mixture and we still have many unsolved problems about dust in ultracool dwarfs.

9. CONCLUDING REMARKS

In general, the purpose of modeling is to understand complicated astronomical phenomena by simple physical principles with least ad-hoc assumptions. In this respect, the model stellar photosphere has been one of the successful cases within the framework of the so-called classical model stellar photosphere. In fact, extensive grids of the classical model photospheres have already been available for most stars including O through M types and they showed reasonable successes in the interpretations and analyses of observed data. We simply extended the method of the model stellar photosphere to effective temperatures as low as 800 K by considering the effect of dust. This could be realized by an additional assumption that only small dust grains (smaller than about 0.01 μm) can be sustained in the photosphere, resulting in a dust cloud deep in the photosphere. We should like to emphasize that this assumption can be regarded as being well supported by the fact that major observations on ultracool dwarfs could be understood reasonably well by our cloudy models based on this assumption.

This fact in turn provides an answer to the problem on how dust forms in the photospheric environment; dust forms and survives rather deep in the photosphere near the dust condensation temperature and not in the cooler surface region. Thus, the major conclusion which we learned from the extensive observations on L and T dwarfs is that the dust cloud should be formed deep in the photospheres of these ultracool dwarfs and this result may be applied to modeling the photosphere with dust in general. We applied this result to the modeling of the photosphrere of substellar brown dwarfs with $T_{\text{eff}} \gtrsim 800$ K in this paper, and showed that the photospheric structure of substellar objects can be modeled by applying the methodology of stellar modeling without incorporating the complexities of the planetary model atmospheres. Probably, our cloudy model may be the most simple model that incorporated the cloud formation, and hopefully provide a clue for unified modeling of the cloudy atmospheres of stars, substellar objects, and giant planets.

I thank Tadashi Nakajima for helpful discussion throughout this work and for reading the manuscript with valuable comments. My thanks are also due to Aleksandra Borysow for making available her codes to compute the absorption coefficients of H₂ CIA and for helpful correspondences. Finally, I am indebted to the referee, Katharina Lodders, for critical reading of the text and for helpful suggestions on the thermochemistry. This work was supported by the grant-in-aid No.11640227 of JSPS, and carried out with the use of the facilities at the Astronomical Data Analysis Center of NAO, which is an inter-university research institute of astronomy operated by Ministry of Education & Science.

A. MOLECULAR OPACITY DATA

A.1. Infrared Bands of H₂O

Until recently, we have been using the experimental data for the straight mean absorption cross-sections and the mean line separation by Ludwig (1967). In the present work, the mean absorption

cross-sections over 25 cm⁻¹ interval are generated from the HITEMP database (Rothman 1997), which is a high temperature adjunct to the well known HITRAN database for atmospheric lines (Rothman et al. 1998). As to the mean line separation, we have also been using Ludwig's data, but we found that the resulting spectra based on the band model method using the mean line separation derived from the fine structure parameter by Ludwig (1967) show rather poor agreement with those by the detailed line-by-line method using the HITEMP database. Accordingly, we introduced correction factors to the Ludwig's data so that the spectra based on the band model agree with those by the detailed line-by-line method.

A.2. Infrared Bands of Polyatomic Molecules

Although spectroscopic data at low temperatures are relatively well known for some polyatomic molecules thanks to the recent spectroscopic databases such as HITRAN (Rothman et al. 1998) and GEISA (Jacquinot-Husson et al. 1999), little is known on spectroscopic properties at elevated temperatures except for H₂O. Thus, only practical approach may be to apply the band model in its most simple form - JOLA - based on the rigid-rotator harmonic oscillator model (Tsuji 1994). Even the application of this simple method is not necessarily easy because of the lack of the intensity data for some bands.

CH₄: This spherical top molecule has 4 fundamentals, of which ν_3 and ν_4 are infrared active (but ν_1 and ν_2 are also weakly active). We have considered 14 band systems for which spectroscopic and intensity data are summarized in Table 3. Unfortunately, some bands are still missing in the region shortward of 1.6 μm . In Fig.14, the resulting absorption coefficient of methane at $T = 296\text{ K}$ based on the band model is compared with that based on the GEISA database. The test is limited to the room temperature at which the GEISA database can be valid, but the band model opacity can in principle be applied to the higher temperatures without limit.

NH₃ and PH₃: These symmetric top molecules have 4 fundamentals for which intensity data are available. But intensity data for overtones are definitely meager and we could include only one overtone for NH₃. Thus, only five and four band systems are included for NH₃ and PH₃, respectively, with the intensity data summarized in Table 3. In addition to these, the pure rotation transitions are included with the known electric dipole moments (Nelson, Lide, & Maryott 1967).

H₂S: This molecule is quite similar to H₂O, but the intensities of the infrared bands are relatively small compared with H₂O. We selected relatively strong 34 band systems from the intensity data evaluated by Senekowitsch et al. (1989). The pure rotation transition is also included.

A.3. Infrared Bands of Diatomic Molecules

The band model parameters - the mean absorption cross-section and the mean line separation - are evaluated from the spectroscopic data for the fundamental, first and second overtone bands of CO, OH, and SiO. The spectroscopic and intensity data are relatively well fixed except for the recent revision of oscillator strengths of SiO bands (Langhoff & Bauschlicher 1993). The band model opacity is tested by comparing the emergent fluxes based on the band model and those evaluated by the use of detailed linelist (Tsuji 1994).

A.4. Electronic Bands of Diatomic Molecules

We evaluated the mean absorption cross-sections and mean line separations for the following 5 molecules. The adopted f -values are summarized in Table 4.

TiO: We considered 8 systems of TiO shown in Table 4. The f -values for δ and ϕ systems are by Davis, Littleton, & Phillips (1986), and those for other 6 systems are based on the direct measurements of the radiative lifetimes by Hedgecock, Naulin, & Costes (1995).

VO: Some details on the Yellow-Green ($C - X$) System are known (Harrington et al. 1971). The importance of VO infrared bands as opacity sources was first noted by Brett (1990), and we apply the f -values of $A - X$ and $B - X$ systems based on the recent lifetime measurements (Karlsson et al. 1997).

FeH: A detailed spectroscopic analysis of the $F - X$ system is done by Phillips et al. (1987). No experimental f -value is known and we applied the *ab initio* results by Langhoff & Bauschlicher (1990). We used the dissociation energy of 1.63 eV by the mass spectrometer experiment (Schultz & Armentrout 1991).

CaH : Intensity and spectroscopic data are not known well, and we had to use an astronomical f -value for $A - X$ system (Mould 1976).

MgH : We apply the *ab initio* f -value for $A - X$ system (Kirby, Saxon, & Liu 1979).

REFERENCES

- Ackerman, A. S., & Marley, M. S. 2001, ApJ, 556, 872
- Alexander, D. R., & Ferguson, J. W. 1994, ApJ, 437, 879
- Allard, F., & Hauschildt, P. H. 1995, ApJ, 445, 433
- Allard, F., Hauschildt, P. H., Alexander, D. R., Tamani, A., & Schweitzer, A. 2001, ApJ, 556, 357
- Allard, F., Hauschildt, P. H., Baraffe, I., & Chabrier, G. 1996, ApJ, 465, L123
- Allende Prieto, C., Lambert, D. L. & Asplund, M. 2001, ApJ, 556, L63
- Anders, E., & Grevesse, N. 1989, Geochim. Cosmochim. Acta, 53, 197
- Auman, J. R. 1969, ApJ, 157, 799
- Bailer-Jones, C. A. L., & Mundt, R. 2001, A&A, 367, 218
- Bauschlicher, C. W., Langhoff, S. R., & Taylor, P. R. 1988, ApJ, 332, 531
- Becklin, E. E., & Zuckerman, B. A. 1988, Nature, 336, 656
- Biémont, E., Baudeoux, M., Kurucz, R. L., Ansbacher, W., & Pinnington, E. H. 1991, A&A, 249, 539
- Blackwell, D. E., Petford, A. D., & Shallis, M. J. 1980, A&A, 82, 249
- Borysow, A., & Frommhold, L. 1989, ApJ, 341, 549
- Borysow, A., & Frommhold, L. 1990, ApJ, 348, L41
- Borysow, A., Frommhold, L., & Moraldi, M. 1989, ApJ, 336, 495
- Borysow, A., Jørgensen, U. G., & Zheng, C. 1997, A&A, 324, 185
- Brett, J. M. 1990, A&A, 231, 440
- Brett, J. M. 1995, A&A, 295, 736
- Brown, L. R. 1982, J. Mol. Spectros., 96, 94
- Brown, L. R. 1988, Appl. Opt., 27, 3275
- Brown, L. R., Farmer, C. B., Rinsland, C. P., & Toth, R. A. 1987, Appl. Opt., 26, 5154
- Burgasser, A. J., et al. 1999, ApJ, 522, L65
- Burgasser, A. J., et al. 2000a, ApJ, 531, L57
- Burgasser, A. J., et al. 2000b, AJ, 120, 1100
- Burgasser, A. J., et al. 2002, ApJ, 564, 421

- Burrows, A. 2001, in Ultracool Dwarfs - New Spectral Types L and T, ed. H. R. A. Jones & I. A. Steele (Springer: Springer-Verlag), 26
- Burrows, A., & Liebert, J. 1993, Rev. Mod. Phys., 65, 301
- Burrows, A., & Sharp, C. M. 1999, ApJ, 512, 843
- Burrows, A., Marley, M. S., & Sharp, C. M. 2000, ApJ, 531, 438
- Burrows, A., et al. 1997, ApJ, 491, 856
- Cerny, D., Bacis, R., Guelachvili, G., & Roux, F. 1978, J. Mol. Spectros., 73, 154
- Chackerian, C. Jr. & Tipping, R. H. 1983, J. Mol. Spectrosc., 99, 431
- Chase, M. W., Davies, C. A., Downey, J. R., Jr., Frurip, D. J., McDonald, R. A., & Syverud, A. N. 1985, J. Phys. Chem. Ref. Data, 14, Supple.1
- Dang-Nhu, M., Pine, A. S., & Robiette, A. G. 1979, J. Mol. Spectros., 77, 57
- Davis, S. P., Littleton, J. E., & Phillips, J. G. 1986, ApJ, 309, 449
- Delfosse, X., et al., 1997, A&A, 327, L25
- Eriksson, T. S., Hjortsberg, A., Niklasson, G. A., & Granqvist, C. G. 1981, Appl. Opt., 20, 2742
- Fegley, B., Jr., & Kornacki, A. S. 1986, Earth Planet. Sci. Lett., 68, 181
- Fegley, B., Jr., & Lodders, K. 1994, Icarus, 110, 117
- Fegley, B., Jr., & Lodders, K. 1996, ApJ, 472, L37
- Geballe, T. R., Kulkarni, S. R., Woodward, C. E., & Sloan, G. C. 1996, ApJ, 467, L101
- Geballe, T. R., et al. 2002, ApJ, 564, 466
- Golden, S. A. 1969, J. Quant. Spectros. Rad. Trans., 9, 1067
- Grevesse, N., Lambert, D. L., Sauval, A. J., van Dishoeck, E. F., Farmer, C. B., & Norton, R. H. 1991, A&A, 242, 488
- Grevesse, N., Lambert, D. L., Sauval, A. J., van Dishoeck, E. F., Farmer, C. B., & Norton, R. H. 1990, A&A, 232, 225
- Grossman, L. 1972, Geochim. Cosmochim. Acta, 36, 597
- Guelachvili, G., De Villeneuve, D., Farrenq, R., Urban, W., & Verges, J. 1983, J. Mol. Spectros., 98, 64
- Gustafsson, B., & Jørgensen, U. G. 1994, A&A Rev., 6, 19
- Harrington, J.A., Seel, R.M., Hebert, G.R., & Nicholls, R.W. 1971, Idendification Atlas of Molecular Spectra, vol.7, *The VO C⁴Σ⁻ - X⁴Σ⁻ Yellow-Green and b⁴Π - X⁴Σ⁻ Red Systems*, York University

- Hasegawa, H., & Kozasa, T. 1988, Prog. Theor. Physics Suppl., No.96, 107
- Hayashi, C., & Nakano, T. 1963, Prog. Theor. Physics, 30, 460
- Hedgecock, I. M., Naulin, C., & Costes, M., 1995, A&A, 304, 667
- Helling, Ch., Oevermann, M., Luttke, M. J. H., Klein, R., & Sedlmayr, E. 2001, A&A, 376, 194
- Holweger, H., Bard, A., Kock, A., & Kock, M. 1991, A&A, 249, 545
- Jacquinet-Husson, N., et al. 1999, J. Quant. Spectros. Rad. Trans., 62, 205
- Jones, H. R. A., & Tsuji, T. 1997, ApJ, 522, L65
- Jones, H. R. A., Longmore, A. J., Jameson, R. F., & Mountain, C. M. 1994, MNRAS, 267, 413
- Karlsson, L., Lindgren, B., Lundvall, C., & Sassenberg, U. 1997, J. Mol. Spectros., 181, 274
- Kim, K. 1985, J. Quant. Spectros. Rad. Trans., 33, 611
- Kirby, K., Saxon, R. P., & Liu, B. 1979, ApJ, 231, 637
- Kirkpatrick, J. D., Beichman, C. A., & Skrutskie, M. F. 1997, ApJ, 476, 311
- Kirkpatrick, J. D., et al. 1999, ApJ, 519, 802
- Kirkpatrick, J. D., et. al. 2000, AJ, 120, 447
- Klynning, L. 1982, Phys. Scrip., 25, 362
- Kumar, S. 1963, ApJ, 137, 1121
- Kurucz, R. L. 1994, Kurucs CD-ROM No.19, Solar Abundance Model Atmospheres for 0,1,2,4,8 km/s,
Smithsonian Astrophysical Observatory
- Langhoff, S. R., & Bauschlicher, C. W. 1990, J. Mol. Spectros., 141, 243
- Langhoff, S. R., & Bauschlicher, C. W. 1993, Chem. Phys. Lett., 211, 305
- Larimer, J. W. 1967, Geochim. Cosmochim. Acta, 31, 1215
- Lavas, F. J., Maki, A. G., & Olson, W. B. 1981, J. Mol. Spectros., 87, 449
- Leggett, S. K., Toomey, D. W., Geballe, T. R., & Brown, R. H. 1999, ApJ, 517, L139
- Leggett, S. K., et al. 2000 ApJ, 536, L35
- Leggett, S. K., et al. 2002, ApJ, 564, 452
- Lenham, A. P., & Treherne, D. M. 1966, in Optical Properties and Electronic Structure of Metal and
Alloys, ed. F. Abelès (Amsterdam: North Holland), 196
- Lierbert, J., Reid, I. N., Burrows, A., Burgasser, A. J., Kirkpatrick, J. D., & Gizis, J. E. 2000, ApJ, 533,
L155

- Linsky, J. L. 1969, ApJ, 156, 989
- Lodders, K. 1999, ApJ, 519, 793
- Lodders, K., & Fegley, B., Jr. 1998, *The Planetary Scientist's Companion* (New York; Oxford Univ. Press)
- Lodders, K., & Fegley, B., Jr. 2002, Icarus, 155, 393
- Lord, H. C., III, 1965, Icarus, 4, 279
- Ludwig, C. B. 1967, Study on Exhaust Plume Radiation Predictions, GDC-DBE67-021, General Dynamics
- Lunine, J. I., Hubbard, W. B., Burrows, A., Wang, Y-P., & Garlow, K. 1989, ApJ, 338, 314
- MaClatchey, R. A., et al. 1973, AFCRL Environmental Research Papers No.434, U. S. Goverment Printing Office
- Margolis, J. S. 1988, Appl. Opt., 27, 4038
- Marley, M. S., Saumon, D., Guillot, T., Freedman, R., Hubbard, W. B., Burrows, A., & Lunine, J. I. 1996, Science, 272, 1919
- Marley, M. S., Seager, S., Saumon, D., Lodders, K., Ackerman, A. S., Freedman, R., & Fan, X. 2002, ApJ, 568, 335
- Martín, E. L., Delfosse, X., Basri, G., Goldman, B., Forveille, T., & Zapatero Osorio, M. R. 1999, AJ, 118, 2466
- Martín, E. L., Zapatero Osorio, M. R., & Lehto, H. J. 2001, ApJ, 557, 822
- McKean, D. C., & Schatz, P. N. 1956, J. Chem. Phys., 24, 316
- McLean, I. S., Prato, L., Kim, S. S., Wilcox, M. K., Kirkpatrick, J. D., & Burgasser, A. 2001, ApJ, 561, L115
- Mould, J. 1976, A&A, 48, 443
- Nakajima, T., Tsuji, T., & Yanagisawa, K. 2001, ApJ, 561, L119
- Nakajima, T., Oppenheimer, B. R., Kulkarni, S. R., Golimowski, D. A., Matthews, K., & Durrance, S. T. 1995, Nature, 378, 463
- Nakajima, T., et al. 2000, PASJ, 52, 87
- Nelson, R. D., Jr., Lide, D. R., Jr., & Maryott, A. A. 1967, Selected Values of Electric Dipole Moments for Molecules in the Gas Phase, NSRDS-NBS 10, National Bureau of Standards
- Noll, K. S., Geballe, T. R., & Marley, M. S. 1997, ApJ, 489, L87
- Oppenheimer, B. R., Kulkarni, S. R., Matthews, K., & Nakajima, T. 1995, Science, 270, 1478

- Oppenheimer, B. R., Kulkarni, S. R., Matthews, K., & van Kerkwijk, M. H. 1998, *ApJ*, 502, 932
- Ordal, M.A., Bell, R.J., Alexander, R. W., Jr. Newrence, L.A., & Query, M. R. 1988, *Appl. Opt.*, 27, 1203
- Ossenkopf, V., Hennings, Th., & Mathis, J. S. 1992, *A&A*, 261, 567
- Partridge, H., & Schwenke, D. W. 1997, *J. Chem. Phys.*, 106, 4618
- Phillips, J. G., Davis, S. P., Lindgren, B., & Balfour, W. J. 1987, *ApJS*, 65, 721
- Pine, A. S., & Dang-Nhu, M. 1993, *J. Quant. Spectros. Rad. Trans.*, 50, 565
- Reid, I. N., Burgasser, A. J., Cruz, K. L., Kirkpatrick, J. D., & Gizis, J. E. 2001, *AJ*, 121, 1710
- Restelli, G., & Cappellani, F. 1982, *Chem. Phys. Letters*, 92, 439
- Rothman, L. S. 1997, High-Temperature Molecular Spectroscopic Database (CD-ROM) (Andover: ON-TAR Co.)
- Rothman, L. S., et al. 1998, *J. Quant. Spectros. Rad. Trans.*, 60, 665
- Saumon, D., Bergeron, P., Lunine, J. I., Hubbard, W. B., & Burrows, A. 1994, *ApJ*, 424, 333
- Schultz, R. H., & Armentrout, P. B. 1991, *J. Chem. Phys.*, 94, 2262
- Senekowitsch, J., Carter, S., Zilch, A., Werner, H-J., Handy, N.C., & Rosmus, P. 1989, *J. Chem. Phys.*, 90, 783
- Sharp, C. M., & Huebner W. F. 1990, *ApJS*, 72, 417
- Simon, D. A., & Tokunaga, A. T. 2002, *PASP*, 114, 169
- Strauss, M. A., et al. 1999, *ApJ*, 522, L61
- Testi, L., et al. 2001, *ApJ*, 552, L147
- Tinney, C. G. 1999, *Nature*, 397, 37
- Tinney, C. G., Mould, J. R., & Reid, I. N. 1993, *AJ*, 105, 1045
- Tipping, R. H., & Chackerian, C., Jr. 1981, *J. Mol. Spectros.*, 88, 352
- Tokunaga, A. T., Simon, D. A., & Vacca, W. D. 2002, *PASP*, 114, 180
- Tsuji, T. 1969, in Low Luminosity Stars, ed. S. S. Kumar (New York: Gordon & Breach Sci. Pub.), 457
- Tsuji, T. 1973, *A&A*, 23, 411
- Tsuji, T. 1984, *A&A*, 134, 24
- Tsuji, T. 1994, in Molecules in Stellar Environment, ed. U. G. Jørgensen (Berlin: Springer-Verlag), 79

- Tsuji, T. 2000, in Very Low-Mass Stars and Brown Dwarfs, ed. R. Rebolo & M. R. Zapatero-Osorio (New York: Cambridge Univ. Press), 156
- Tsuji, T. 2001, in Ultracool Dwarfs - New Spectral Types L and T, ed. H. R. A. Jones & I. A. Steele (Berlin: Springer-Verlag), 9
- Tsuji, T., & Ohnaka, K. 1995a, in Elementary Processes in Dense Plasmas, ed. S. Ichimaru & S. Ogata (Reading: Addison-Wesley), 193
- Tsuji, T., & Ohnaka, K. 1995b, in ASP Conf. Ser. 78, Astrophysical Applicaions of Powerful New Databases, ed. S. J. Adelman & W. L. Wiese (San Francisco: ASP), 69
- Tsuji, T., Ohnaka, K., & Aoki, W. 1996a, A&A, 305, L1
- Tsuji, T., Ohnaka, K., & Aoki, W. 1999, ApJ, 520, L119
- Tsuji, T., Ohnaka, K., Aoki, W., & Nakajima, T. 1996b, A&A, 308, L29
- Tsvetanov, Z. I., et al. 2000, ApJ, 531, L61
- Van de Hulst, H. C. 1957, Light Scattering by Small Particles (New York: John Wiley & Sons Inc.)
- Viti, S., Tennyson, J., & Polyansky, O. L. 1997, MNRAS, 287, 79
- Wiese, W. L., Smith, M. W., & Miles, B. M. 1969, Atomic Transition Probabilities Volume II Sodium through Calcium, U. S. Government Printing Office
- Zheng, C., & Borysow, A. 1995, ApJ, 441, 960

Table 1: CHEMICAL COMPOSITION^a

Atomic No.	El.	$\log A_{\text{El}}$	Atomic No.	El.	$\log A_{\text{El}}$
1	H	12.00	20	Ca	6.36
2	He	10.99	21	Sc	3.10
3	Li	3.31	22	Ti	4.99
4	Be	1.15	23	V	4.00
5	B	2.60	24	Cr	5.67
6	C	8.60 ^b	25	Mn	5.39
7	N	8.00 ^c	26	Fe	7.51 ^e
8	O	8.92 ^d	28	Ni	6.25
9	F	4.56	29	Cu	4.21
11	Na	6.33	35	Br	2.63
12	Mg	7.58	37	Rb	2.69
13	Al	6.47	38	Sr	2.90
14	Si	7.55	39	Y	2.24
15	P	5.45	40	Zr	2.60
16	S	7.21	53	I	1.51
17	Cl	5.50	56	Ba	2.13
19	K	5.12	57	La	1.22

^abased on Anders & Grevesse (1989) except for those footnoted

^bGrevesse et al.(1991)

^cGrevesse et al.(1990)

^drecent value of 8.69 by Allende Prieto et al.(2001) is also tried in some models

^eBiémont et al.(1991); Holweger et al.(1991)

Table 2: COLOR INDECES AND EFFECTIVE TEMPERATURES

Sp. type	$J - K$	T_{eff}	$J - H$	T_{eff}	$H - K$	T_{eff}	$T_{\text{eff}}(\text{mean})$
L0	1.0	1970 K	0.5	2150 K	0.45	1960 K	2030 K
L3	1.5	1780	0.85	1770	0.7	1740	1760
L6	1.8	1520	1.0	1510	0.8	1540	1520
L9	1.5	1450	0.9	1450	0.55	1440	1450
T2	0.8	1320	0.5	1280	0.25	1340	1310
T5	-0.05	1050	-0.05	1110	0.0	800	990

Table 3: INTENSITY DATA OF POLYATOMIC MOLECULES

Molecule	$n_1 n_2 n_3 n_4$	$\omega(\text{cm}^{-1})$	$f_{n_1 n_2 n_3 n_4}^0$	Ref.
NH_3	0 1 0 0	950	2.39×10^{-5}	1
	0 0 0 1	1630	4.65×10^{-6}	1
	0 2 0 0	1739	4.72×10^{-8}	2
	1 0 0 0	3337	1.03×10^{-6}	3
	0 0 1 0	3448	6.04×10^{-7}	3
PH_3	0 1 0 0	992	3.45×10^{-6}	4
	0 0 0 1	1122	4.29×10^{-6}	4
	1 0 0 0	2323	1.09×10^{-5}	4
	0 0 1 0	2328	1.09×10^{-5}	4
CH_4	0 0 0 1	1311	5.65×10^{-6}	5
	0 1 0 0	1533	1.01×10^{-7}	6
	0 0 0 2	2622	1.13×10^{-7}	6
	0 1 0 1	2844	9.05×10^{-7}	6
	1 0 0 0	2916	1.31×10^{-9}	7
	0 0 1 0	3019	1.21×10^{-5}	8
	0 2 0 0	3067	3.85×10^{-8}	7
	0 0 0 3	3932	3.43×10^{-8}	9
	0 1 0 2	4155	3.43×10^{-8}	9
	1 0 0 1	4227	3.16×10^{-7}	10
	0 0 1 1	4330	4.61×10^{-7}	7
	0 1 1 0	4553	7.07×10^{-8}	7
	0 0 1 2	5641	1.39×10^{-9}	7
	2 0 0 0	5832	7.49×10^{-8}	11
	1 0 1 0	5935	7.49×10^{-8}	11
	0 0 2 0	6039	7.49×10^{-8}	12

References. — (1) Kim 1985; (2) Brown et al. 1987; (3) Pine & Dang-Nhu 1993; (4) McKean & Schatz 1956; (5) Restelli & Cappellani 1982; (6) MaClatchey et al. 1973; (7) Rothman et al. 1998; (8) Dang-Nhu et al. 1979; (9) Brown 1988; (10) Brown 1982; (11) f value is assumed to be the same as that of $2\nu_3$ band; (12) Margolis 1988.

Table 4: THE f -VALUES OF THE ELECTRONIC BANDS

Molecule	Transition	ω_{00} (cm $^{-1}$)	f_{00}	Ref.
TiO	$A^3\Phi-X^3\Delta(\gamma)$	14,163	0.112	1
	$B^3\Pi-X^3\Delta(\gamma')$	16,219	0.100	1
	$C^3\Delta-X^3\Delta(\alpha)$	19,424	0.073	1
	$E^3\Pi-X^3\Delta(\epsilon)$	11,885	0.012	1
	$b^1\Pi-a^1\Delta(\delta)$	11,319	0.039	2
	$c^1\Phi-a^1\Delta(\beta)$	17,890	0.26	1
	$f^1\Delta-a^1\Delta$	19,140	0.061	1
	$b^1\Pi-d^1\Sigma(\phi)$	9,100	0.03	2
VO	$A^4\Pi-X^4\Sigma^-$	9,494	0.009	3
	$B^4\Pi-X^4\Sigma^-$	12,606	0.16	3
	$C^4\Sigma^--X^4\Sigma^-$	17,420	0.009	4
FeH	$F^4\Delta-X^4\Delta$	9,995	0.013	5
CaH	$A^2\Pi-X^2\Sigma$	14,394	0.059	6
	$B^2\Pi-X^2\Sigma$	15,754	0.113	7
MgH	$A^2\Pi-X^2\Sigma^+$	19,288	0.161	8

References. — (1) Hedgecock et al. 1995; (2) Davis et al. 1986; (3) Karlsson 1997; (4) Harrington et al. 1970; (5) Langhoff & Bauschlicher 1990; (6) Mould 1976; (7) Klynning 1982; (8) Kirby et al. 1979.

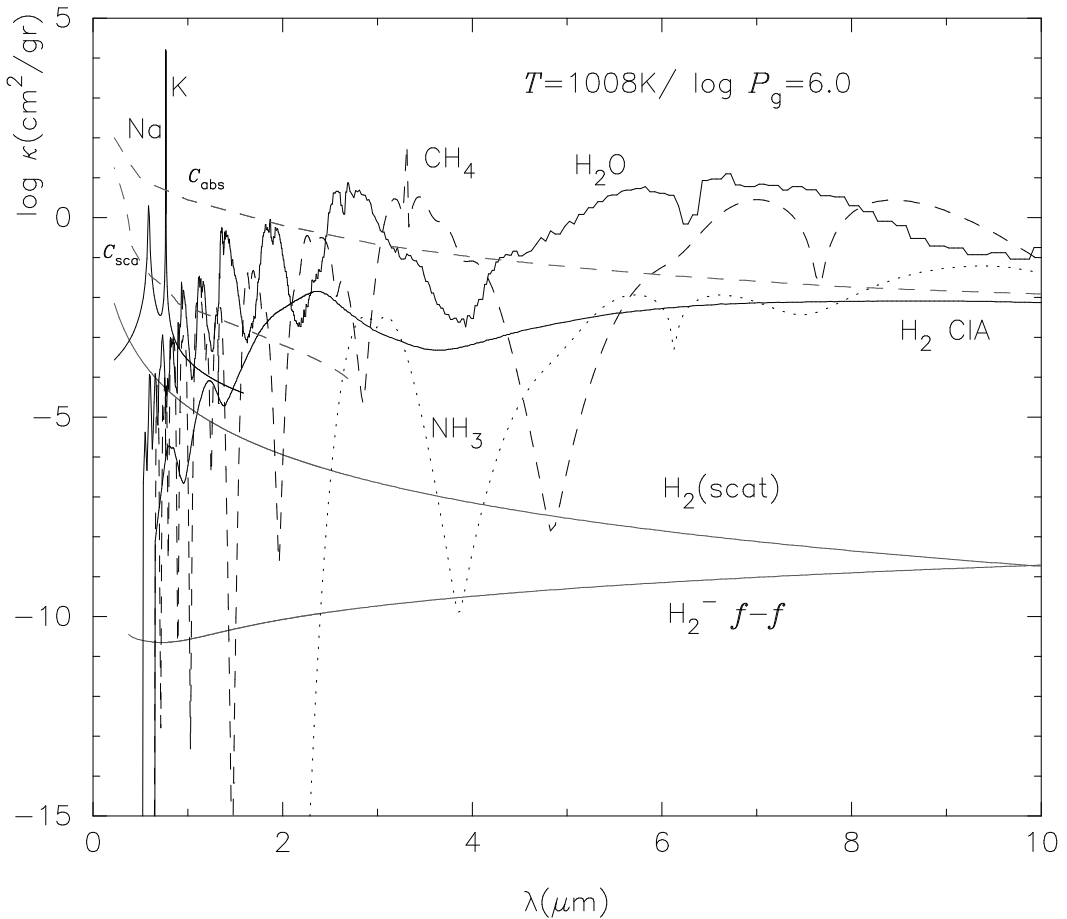


Fig. 1.— The extinction coefficients (per gram of stellar material) of major opacity sources in the solar composition mixture at $T = 1,008\text{K}$ and $\log P_g = 6.0$. The absorption and scattering coefficients of iron particles ($r_{\text{gr}} = 0.01\mu\text{m}$) are also shown by C_{abs} and C_{sca} , respectively, although dust grains may have segregated from the gaseous mixture and may not be effective as sources of opacity at the physical condition shown here.

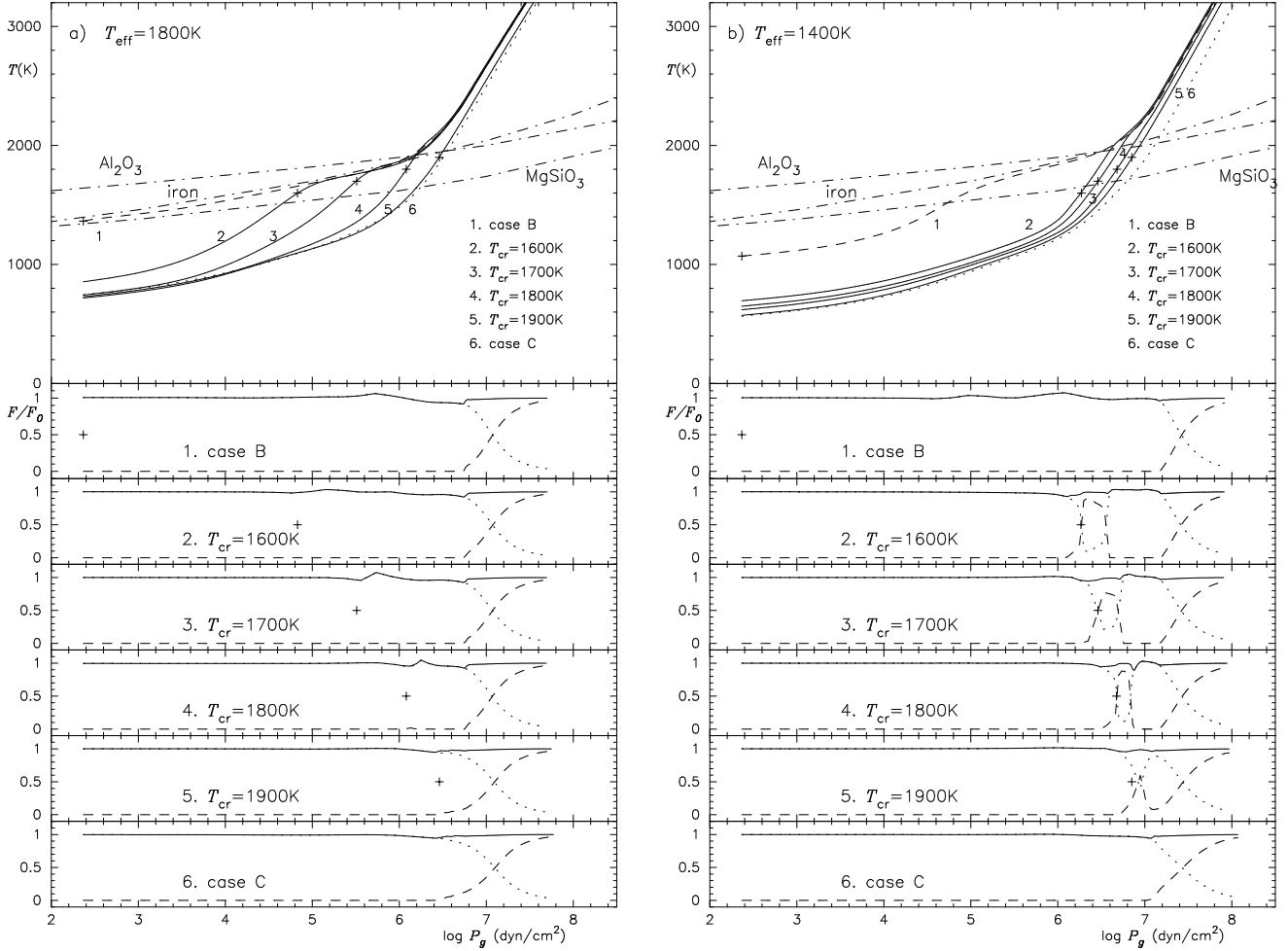


Fig. 2.— a) Non-grey model photospheres of $T_{\text{eff}} = 1800\text{K}$ ($\log g = 5.0$, $v_{\text{micro}} = 1 \text{ km s}^{-1}$ and the solar metallicity) are shown in the upper panel for six values of the critical temperatures; $T_{\text{cr}} = T_0$ (case B), 1600, 1700, 1800, 1900, and T_{cond} (case C). The solid lines illustrate the cloudy models with T_{cr} 's indicated and the plus signs denote the upper boundary of the cloud (where $T = T_{\text{cr}}$). The dashed and dotted lines show the extreme limiting cases B and C, respectively. The dot-dashed curves are the dust condensation lines for corundum, iron, and enstatite. The lower six panels show the radiative, convective, and total fluxes normalized by $\sigma T_{\text{eff}}^4 / \pi$ by the dotted, dashed, and solid lines, respectively, for six values of the critical temperatures. b) The same as a) but for the case of $T_{\text{eff}} = 1400\text{K}$. Note a drastic change of the convective structure compared with the case of $T_{\text{eff}} = 1800\text{K}$.

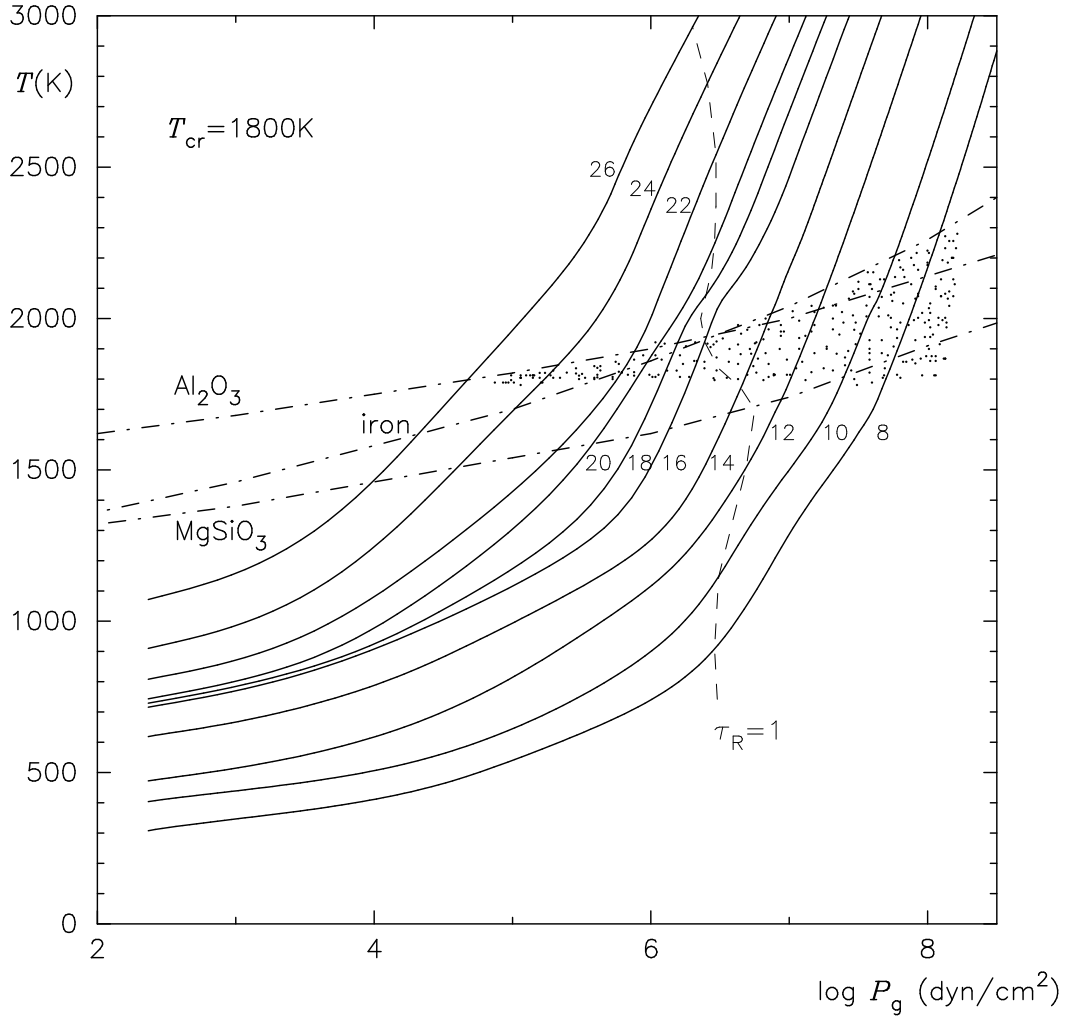


Fig. 3.— The cloudy model photospheres with $T_{\text{cr}} = 1800 \text{ K}$ for T_{eff} from $= 800 \text{ K}$ to 2600 K by a step of $\Delta T_{\text{eff}} = 200 \text{ K}$ ($\log g = 5.0$, $v_{\text{micro}} = 1 \text{ km s}^{-1}$ and the solar metallicity). The numbers attached are T_{eff} in units of 100 Kelvin and the cloud zone is shown by the dotted area. The locus where the Rosseland mean optical depth unity is shown by the dashed line. Some details of the radiative/convective structures are shown in Fig.5.

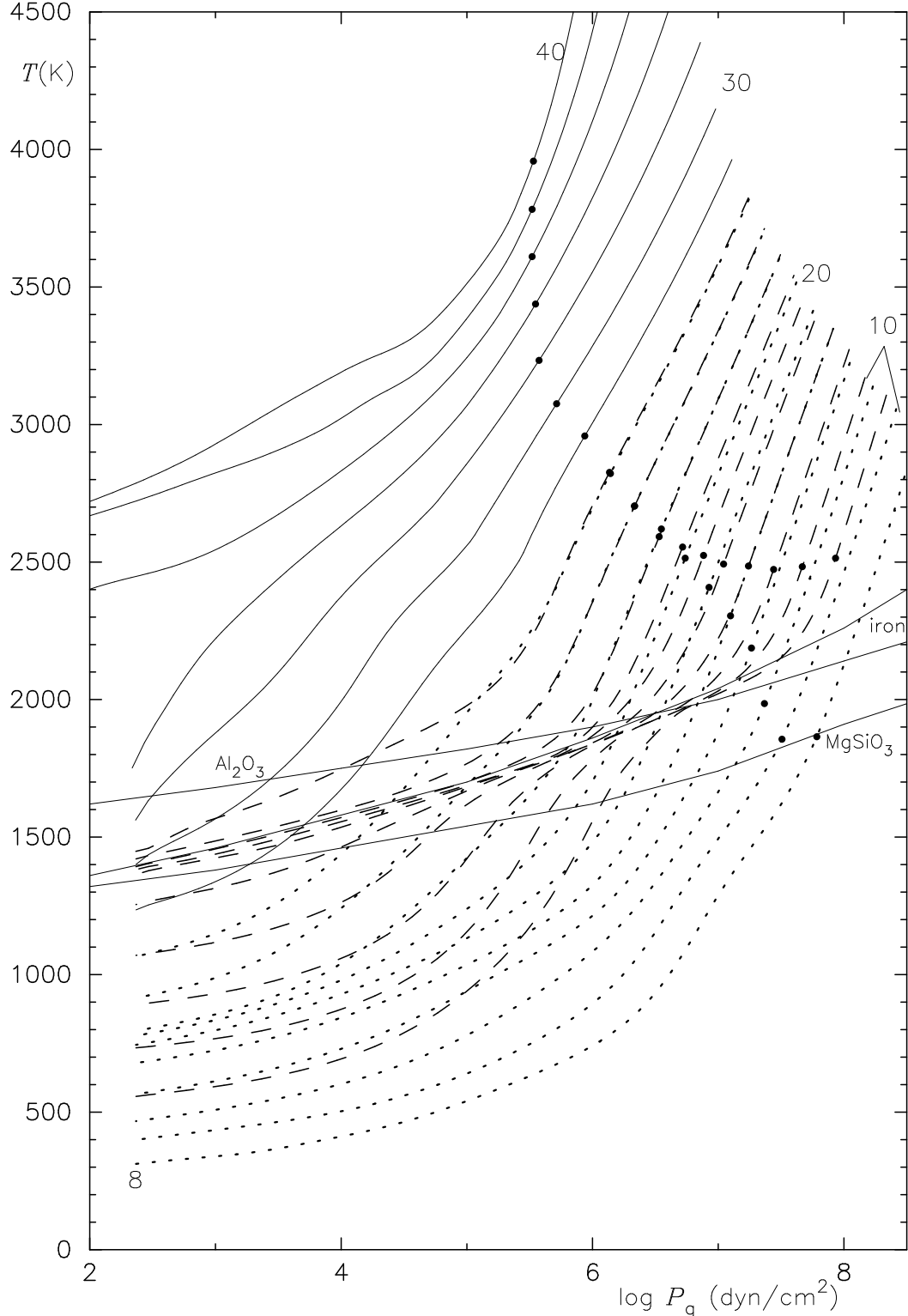


Fig. 4.— The extreme limiting cases of dusty (case B) and dust segregated (case C) models are shown by the dashed and dotted lines, respectively, for T_{eff} from 800 K to 2600 K by a step of $\Delta T_{\text{eff}} = 200$ K. The case C models are extended to the dust-free regime with T_{eff} between 2800 K and 4000 K and shown by the solid lines. The filled circles are where $F_{\text{rad}} = F_{\text{cnv}}$ and denote the transition from the radiative to convective zones. Other details are the same as the Fig. 3 legend.

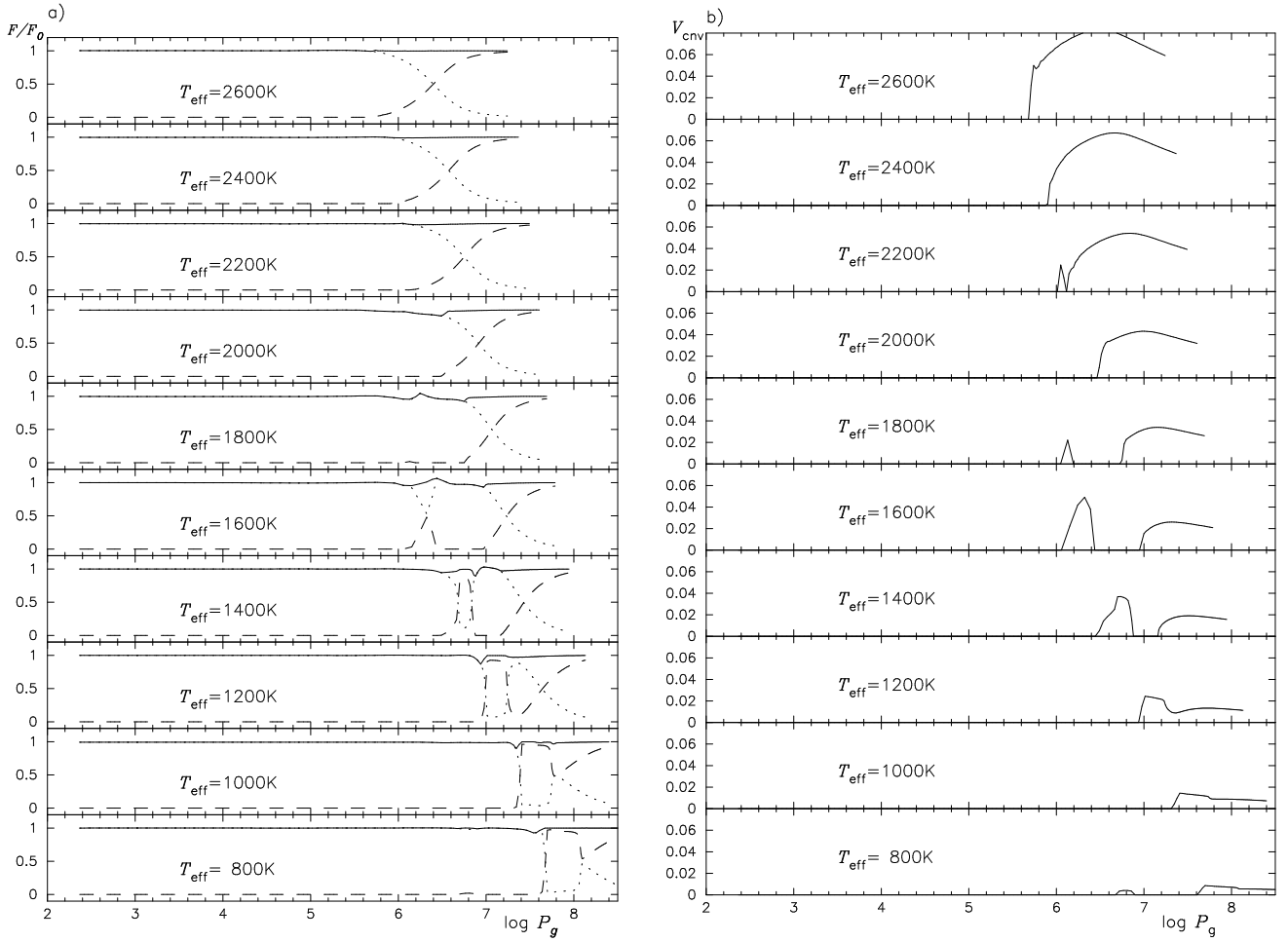


Fig. 5.— a) The radiative, convective, and total fluxes normalized by $\sigma T_{\text{eff}}^4/\pi$ are shown by the dotted, dashed, and solid lines, respectively, for the cloudy model photospheres with $T_{\text{cr}} = 1800\text{ K}$ for T_{eff} from 800 K to 2600 K. b) The convective velocity in units of km s^{-1} for the same models shown in a).

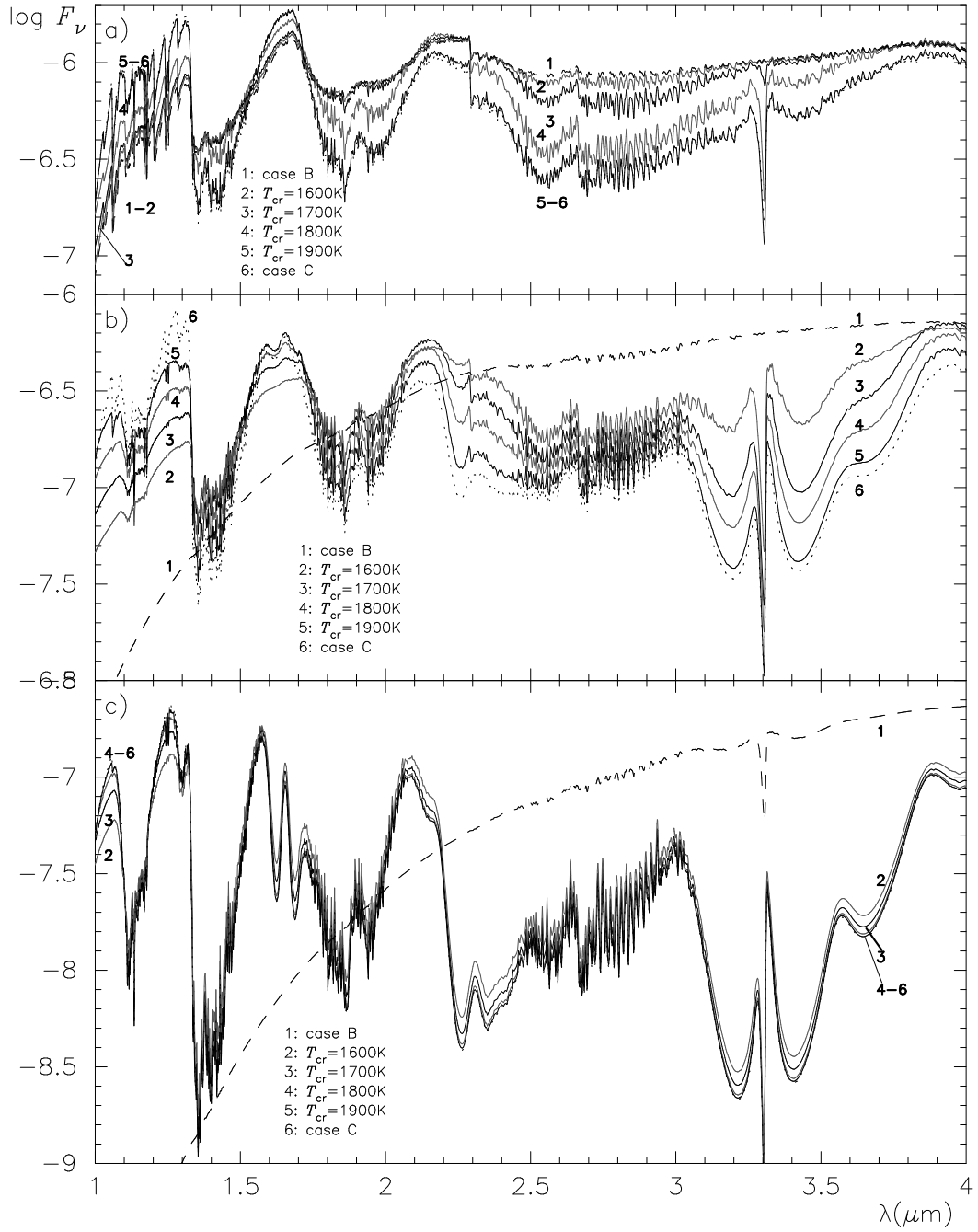


Fig. 6.— a) Predicted spectra from the models of the same T_{eff} ($\log g = 5.0$, $v_{\text{micro}} = 1 \text{ km s}^{-1}$ and the solar metallicity) for six values of the critical temperatures; $T_{\text{cr}} = T_0$ (case B), 1600, 1700, 1800, 1900, and T_{cond} (case C). The dashed, solid (black and grey), and dotted lines illustrate model B, cloudy models, and model C, respectively. a) $T_{\text{eff}} = 1800\text{K}$. b) $T_{\text{eff}} = 1400\text{K}$. c) $T_{\text{eff}} = 1000\text{K}$.

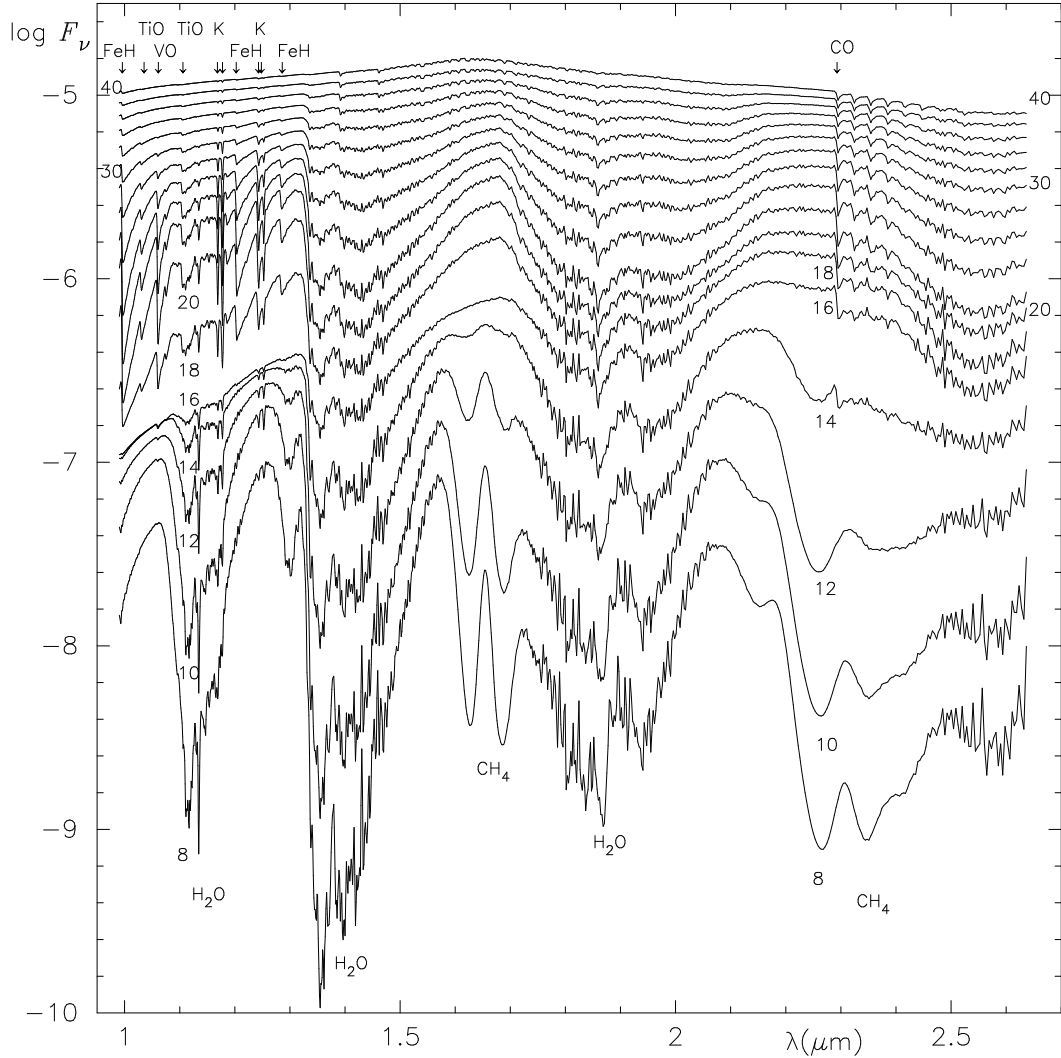


Fig. 7.— The spectra between 1.0 and 2.6 μm predicted from the cloudy models with $T_{\text{cr}} = 1800 \text{ K}$ for T_{eff} between 800 and 2600 K and those from the dust-free models for T_{eff} between 2800 and 4000 K. The step of T_{eff} is 200 K, and T_{eff} in units of 100 Kelvin are indicated on some spectra.

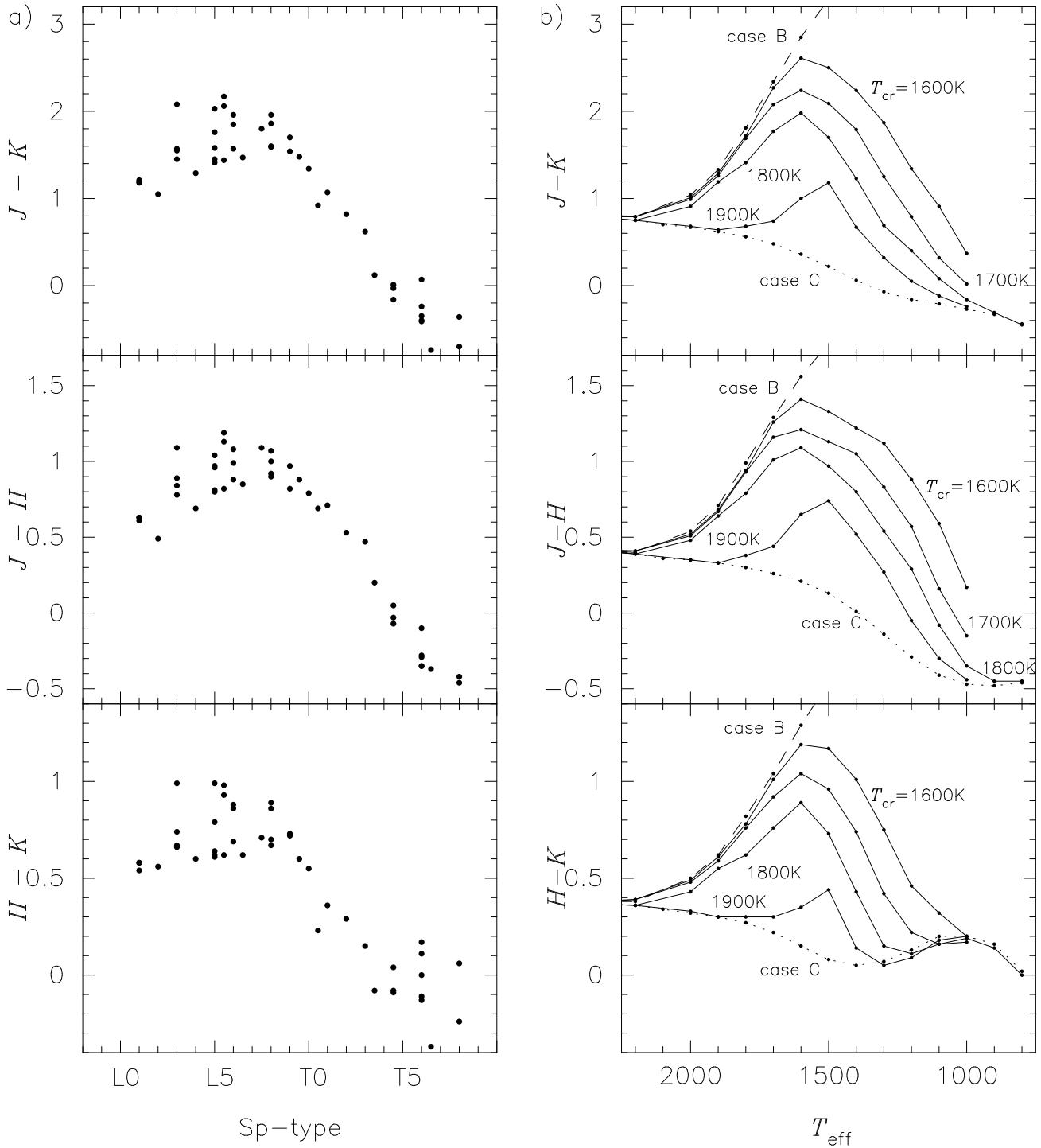


Fig. 8.— a) The observed $J - K$, $J - H$, and $H - K$ colors (Leggett et al. 2002) are plotted against the spectral types (Geballe et al. 2002) in the top, middle, and bottom panels, respectively. b) The predicted $J - K$, $J - H$, and $H - K$ colors are plotted against T_{eff} in the top, middle, and bottom panels, respectively. The results based on the dusty models (case B), cloudy models of $T_{\text{cr}} = 1600, 1700, 1800$, & 1900 K, and dust-segregated models (case C) are shown by the dashed, solid, and dotted lines, respectively.

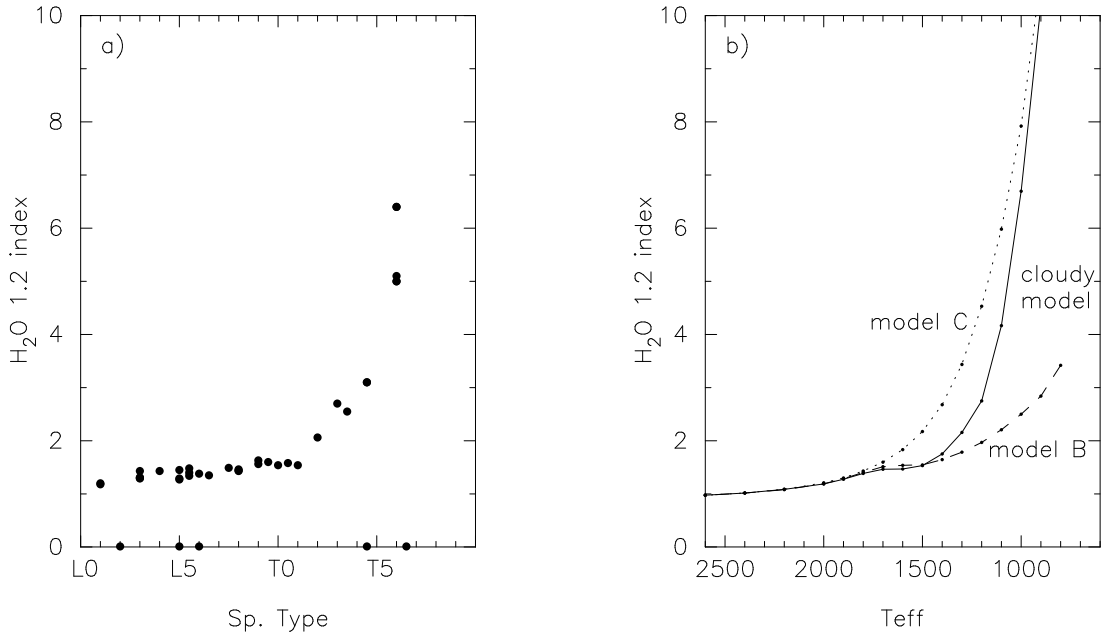


Fig. 9.— a) The observed H_2O 1.2 μm index defined as $F_{\lambda}(1.26-1.29\mu\text{m})/F_{\lambda}(1.13-1.16\mu\text{m})$ by Geballe et al. (2002) is plotted against their Sp-type. b) The predicted H_2O 1.2 μm indices based on the case B models, cloudy models of $T_{\text{cr}} = 1800$ K, and case C models are plotted against T_{eff} by the dashed, solid, and dotted lines, respectively.

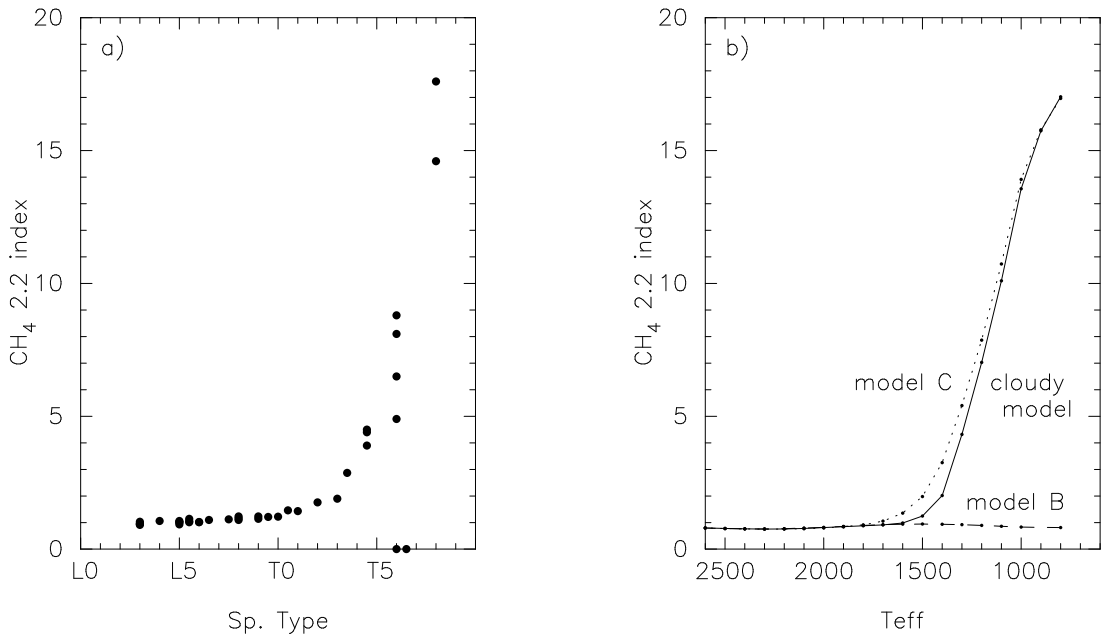


Fig. 10.— a) The observed CH_4 2.2 μm index, $F_{\lambda}(1.26-1.29\mu\text{m})/F_{\lambda}(1.13-1.16\mu\text{m})$ by Geballe et al. (2002) is plotted against their Sp-type. b) The predicted CH_4 2.2 μm indices based on the case B models, cloudy models of $T_{\text{cr}} = 1800$ K, and case C models are plotted against T_{eff} by the dashed, solid, and dotted lines, respectively.

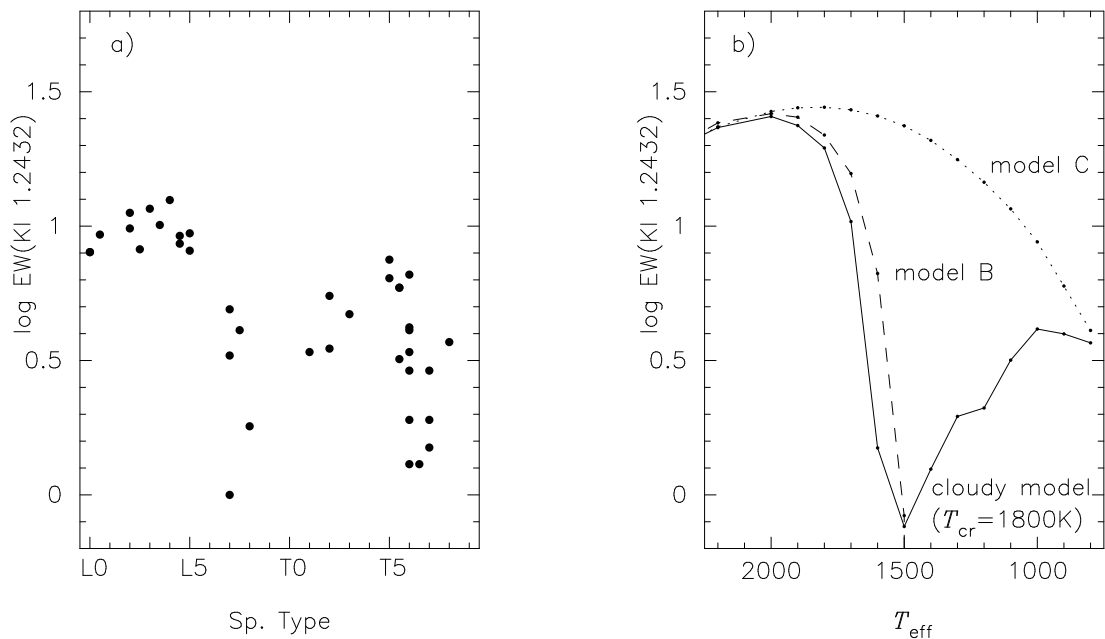


Fig. 11.— a) The observed pseudo-EW's of K I $1.2432\text{ }\mu\text{m}$ given by Burgasser et al. (2002) are plotted against their Sp-type. b) The EW's of K I $1.2432\text{ }\mu\text{m}$ measured on the predicted spectra based on the case B models, cloudy models of $T_{\text{cr}} = 1800\text{K}$, and case C models are plotted against T_{eff} 's of the models by the dashed, solid, and dotted lines, respectively..

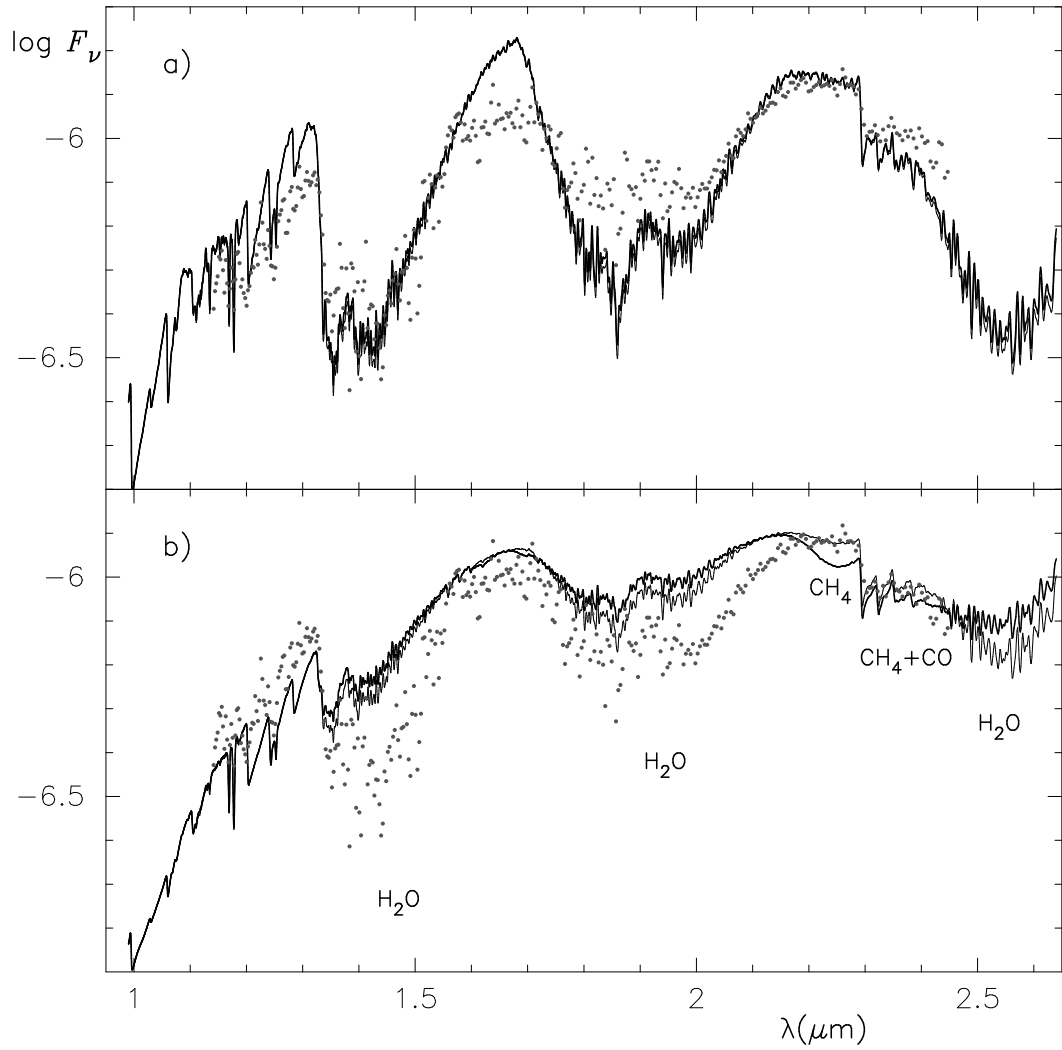


Fig. 12.— Comparison of the observed infrared spectrum of GD 165B (Jones et al. 1994) shown by the dots with the predicted ones based on the cloudy models of $T_{\text{cr}} = 1800\text{ K}$ and $T_{\text{eff}} = 1800\text{ K}$, showing the effects of the oxygen abundance as well as of the silicate formation on the molecular abundances. a) The case of the high oxygen abundance ($\log A_O = 8.92$ as in the Table 1) is shown with and without the effect of silicate formation on the molecular abundances by the heavy and thin solid lines, respectively. b) The same as in a) but for the case of the low oxygen abundance ($\log A_O = 8.69$ by Allende Prieto et al. 2001).

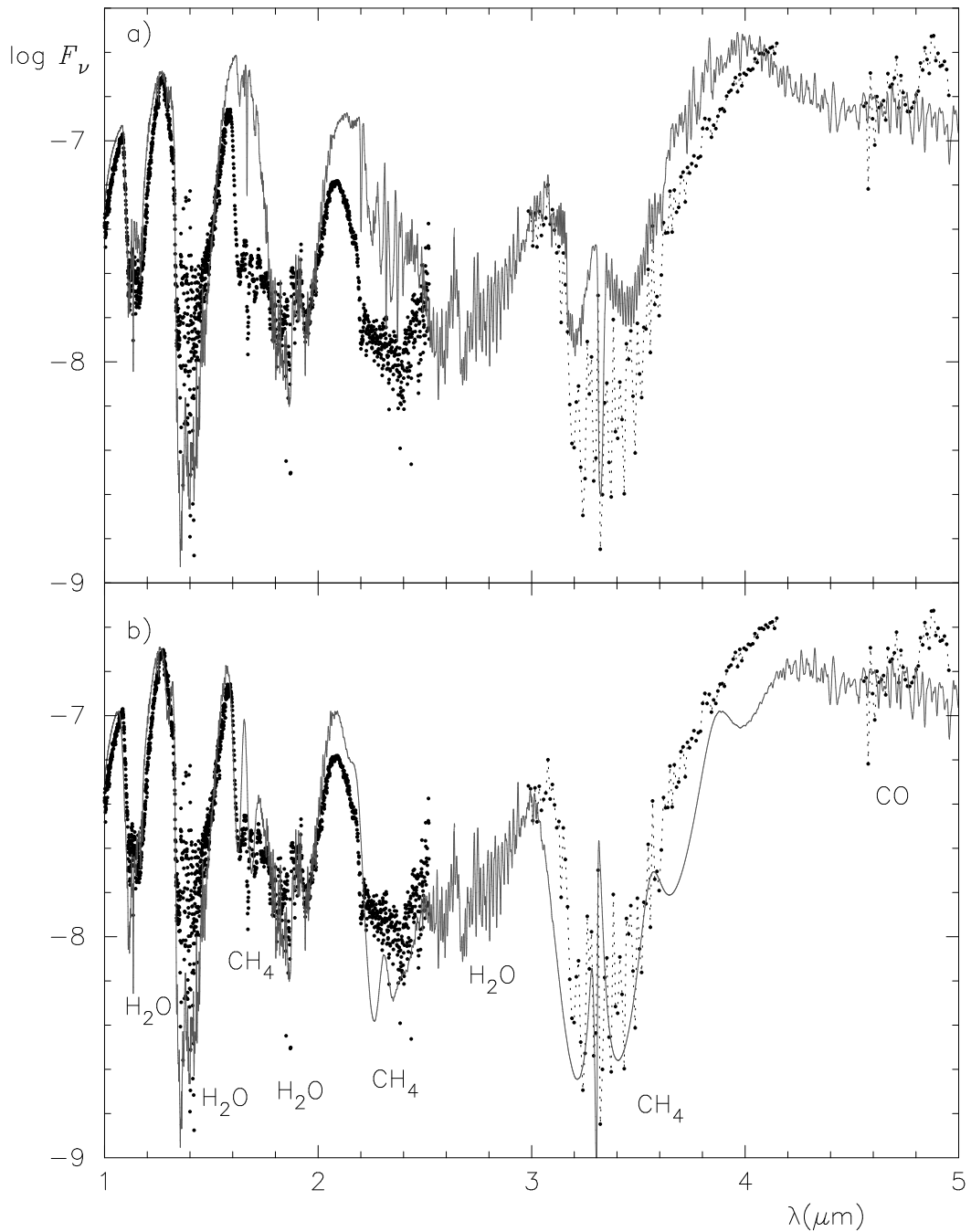


Fig. 13.— a) Comparison of the observed infrared spectrum of Gl 229B (Geballe et al. 1996; Oppenheimer et al. 1998; Leggett et al. 1999) with the predicted one using the GEISA linelist of methane on the cloudy model of $T_{\text{eff}} = 1000$ K with $T_{\text{cr}} = 1800$ K. b) Comparison of the same observed spectrum of Gl 229B with the predicted one using the band model opacity of methane on the same cloudy model of $T_{\text{eff}} = 1000$ K with $T_{\text{cr}} = 1800$ K. The observed data and predicted spectra are shown by the dots and grey lines, respectively.

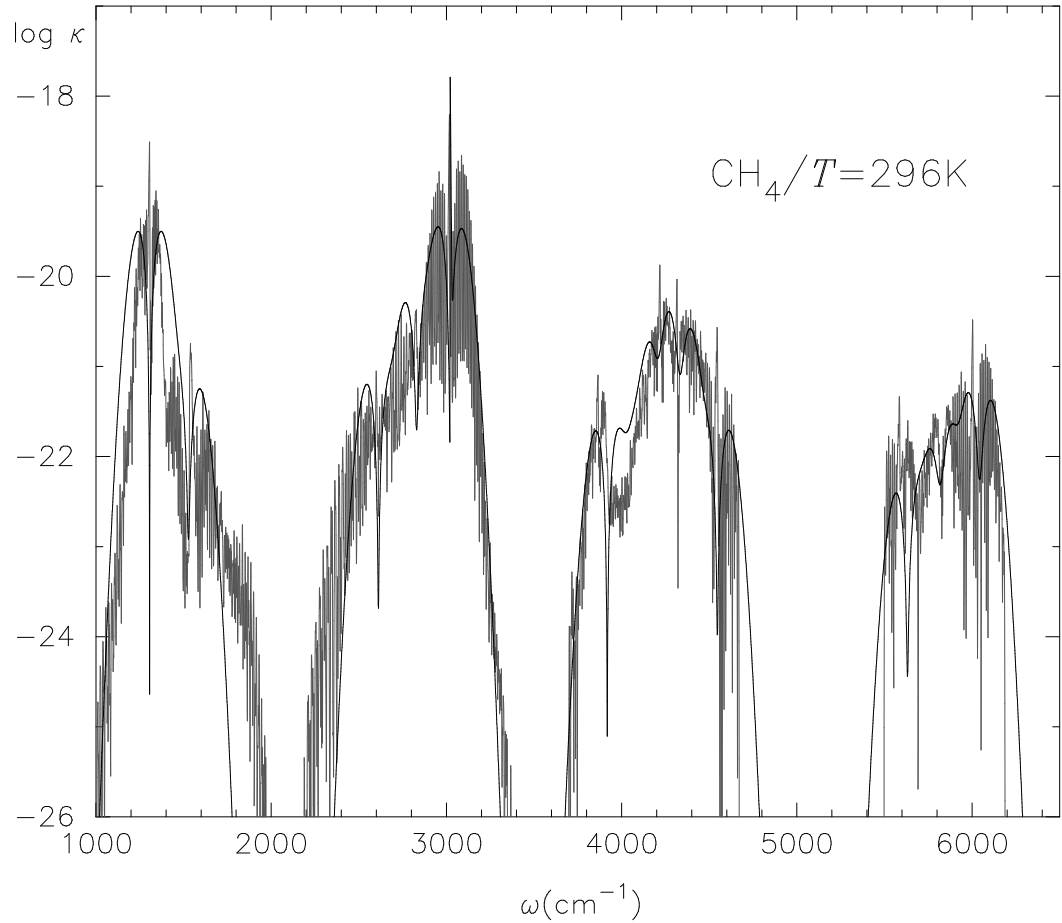


Fig. 14.— Absorption cross-sections (cm^2) of methane at $T = 296\text{K}$ evaluated with the use of the GEISA database and with the band model are shown by the grey and black lines, respectively.